THE EFFECT OF INFILL WALLS ON THE SEISMIC PERFORMANCE OF BOUNDARY COLUMNS IN REINFORCED CONCRETE FRAMES

A THESIS SUBMITTED TO
THE GRADUATE SCHOOL OF NATURAL AND APPLIED SCIENCES
OF
MIDDLE EAST TECHNICAL UNIVERSITY

BY

AKSEL FENERCİ

IN PARTIAL FULFILLMENT OF THE REQUIREMENTS
FOR
THE DEGREE OF MASTER OF SCIENCE
IN
CIVIL ENGINEERING

SEPTEMBER 2013

Approval of the thesis:

THE EFFECT OF INFILL WALLS ON THE SEISMIC PERFORMANCE OF BOUNDARY COLUMNS IN REINFORCED CONCRETE FRAMES

submitted by **AKSEL FENERCİ** in partial fulfillment of the requirements for the degree of **Master of Science in Civil Engineering Department, Middle East Technical University** by

Prof. Dr. Canan Özgen _____
Dean, Graduate School of **Natural and Applied Sciences**

Prof. Dr. Ahmet Cevdet Yalçıner _____
Head of Department, **Civil Engineering**

Prof. Dr. Barış Binici _____
Supervisor, **Civil Engineering Dept., METU**

Examining Committee Members:

Prof. Dr. Güney Özcebe _____
Civil Engineering Dept., TED University

Prof. Dr. Barış Binici _____
Civil Engineering Dept., METU

Prof. Dr. Ahmet Yakut _____
Civil Engineering Dept., METU

Assoc. Prof. Dr. Erdem Canbay _____
Civil Engineering Dept., METU

Assoc. Prof. Dr. Altuğ Erberik _____
Civil Engineering Dept., METU

Date: 4.09.2013

I hereby declare that all information in this document has been obtained and presented in accordance with academic rules and ethical conduct. I also declare that, as required by these rules and conduct, I have fully cited and referenced all material and results that are not original to this work.

Name, Last name : AKSEL FENERCİ

Signature :

ABSTRACT

THE EFFECT OF INFILL WALLS ON THE SEISMIC PERFORMANCE OF BOUNDARY COLUMNS IN REINFORCED CONCRETE FRAMES

Fenerci, Aksel

M.Sc., Department of Civil Engineering

Supervisor: Prof. Dr. Barış Binici

September 2013, 67 pages

Reinforced concrete frames with unreinforced masonry infill walls constitute a significant portion of the building stock throughout the world. Infill walls in these buildings are generally considered as non-structural elements and neglected during design and assessment. On the other hand, observations after several earthquakes revealed that infill walls may have detrimental effects on the adjacent frame members. This observation brings out the requirement for further research on the effects of infill walls on the seismic performance of boundary columns. Additionally, current procedures for the design and assessment of such structures should be experimentally tested and validated along with the development of accurate numerical simulation tools is still in need for these purposes.

In this study, seismic behavior of two test specimens which were designed, constructed and tested using the pseudo dynamic testing method in the Structural Mechanics Laboratory of Middle East Technical University are investigated. The two test frames were code conforming and seismically deficient frames. Numerical modeling of the test frames was conducted using DIANA (2008) finite element platform with the available constitutive models. The modeling approach was validated with the experimental results through comparisons. The analysis results are presented for a better understanding of the shear forces transferred from infill walls to the boundary columns. Seismic assessment

of the two frames was conducted using ASCE/SEI 41-06 guidelines and the obtained results were compared to the damage observed during experiments.

It was found that the presence of infill walls greatly altered the strength, stiffness, deformation capacity, ductility and failure mode of the reinforced concrete test frames. Significant amount of shear force transfer caused shear damage on boundary columns and decreased the ductility.

ASCE/SEI 41-06 procedures for seismic assessment of reinforced concrete frames with infill walls are found as unsatisfactory in estimating the observed damage. Use of plastic hinge strains instead of average strain along the member length provided better estimations for boundary column damage levels.

Keywords: Pseudo dynamic testing, unreinforced masonry infill wall, numerical modeling, finite element method, seismic assessment

ÖZ

BETONARME ÇERÇEVELERDE DOLGU DUVARLARIN KENAR KOLONLARIN SİSMİK PERFORMANSINA ETKİSİ

Fenerci, Aksel

Yüksek Lisans, İnşaat Mühendisliği Bölümü

Tez Yöneticisi: Prof. Dr. Barış Binici

Eylül 2013, 67 sayfa

Donatısız dolgu duvarlı betonarme çerçeveler, dünyadaki yapı stoğunun önemli bir kısmını oluşturmaktadır. Bu binalardaki dolgu duvarlar genellikle yapısal olmayan elemanlar olarak değerlendirilmekte ve tasarım ile performans değerlendirilmesinde hesaba katılmamaktadırlar. Öte yandan, birçok deprem, dolgu duvarların hasar verici etkileri olabileceğini göstermiştir. Bu gözlem, dolgu duvarların kenar kolonları üzerindeki etkilerinin daha fazla araştırılması gerekliliğini ortaya çıkarmaktadır. Buna ek olarak, bu gibi yapıların tasarım ve performans değerlendirmesinde kullanılan güncel yöntemler, isabetli simülasyon araçlarının geliştirilmesi ile beraber deneysel olarak test edilmeli ve doğrulanmalıdır.

Bu çalışmada, Orta Doğu Teknik Üniversitesi Yapı Mekaniği Laboratuvarında tasarlanmış, inşa edilmiş ve dinamik benzeri deney yöntemi ile test edilmiş iki adet deney numunesinin sismik davranışları incelenmiştir. Deney çerçeveleri, biri yönetmelik uyumlu, öteki sismik olarak yetersiz iki çerçeveden oluşmaktadır. Deney numunelerinin sayısal modellemesi DIANA (2008) sonlu eleman platformunda, mevcut bünye modelleri kullanılarak yapılmıştır. Modelleme yaklaşımı deneylerle karşılaştırılarak doğrulanmıştır. Analiz sonuçları, dolgu duvarlardan kenar kolonlarına aktarılan kesme kuvvetlerinin daha iyi anlaşılmasını sağlamıştır. Ayrıca, iki deney çerçevesinin sismik performans değerlendirmesi ASCE/SEI 41-06 prensiplerine göre yapılmış ve elde edilen sonuçlar deneyde gözlenen hasarla karşılaştırılmıştır.

Dolgu duvarların varlığının betonarme çerçevelerin mukavemet, rijitlik, deformasyon kapasitesi, süneklik ve göçme şeklini önemli ölçüde değiştirdiği bulunmuştur. Dolgu duvarlardan kenar kolonlarına aktarılan dikkate değer miktarda kesme kuvveti, kesme hasarına neden olup, sünekliği azaltmaktadır.

Dolgu duvarlı betonarme çerçevelerin sismik performans değerlendirmesi için önerilen ASCE/SEI 41-06 yöntemleri, gözlenen hasarı tahmin etmekte yetersiz bulunmuştur. Mevcut yöntem güvensiz sonuçlar vermektedir. Eleman boyunca ortalama birim şekildeğiştirme kullanmaktansa, plastik mafsal boyunca ortalama şekildeğiştirme kullanmak, kolon hasar seviyelerini belirlemede daha güvenli tahminler vermektedir.

Anahtar Kelimeler: Dinamik benzeri deney yöntemi, donatısız tuğla dolgu duvar, sayısal modelleme, sonlu eleman yöntemi, performans değerlendirmesi.

To my family…

ACKNOWLEDGEMENTS

The research presented in this thesis was conducted under the supervision of Prof. Dr. Barış Binici. I would like to express my gratitude to him above all others. He has been the best supervisor and mentor a student could ask for. His extraordinary insight and warm attitude provided motivation in every stage of this study. I will carry the honor of working with him my whole life.

I would also like to thank Prof. Dr. Güney Özcebe for his support and guidance during my graduate study and academic life. I am grateful for his fatherly attitude and good intentions. He will always be more than a professor to me.

I also owe thanks to my professors back in METU Northern Cyprus Campus, Prof. Dr. Kağan Tuncay, Asst. Prof. Dr. Ozan Cem Çelik and Asst. Prof. Dr. Zehra Çağnan. Their guidance and extraordinary teaching abilities helped me become the person who I am now. I would like to express my deepest gratitude to Prof. Dr. Kağan Tuncay. His enthusiasm and scientific perspective literally changed my life.

My deepest thanks will go to my family. I cannot possibly express the importance of my mother, Prof. Dr. Tülay Fenerci to me. She has been the most loving, caring, patient mother and she has always been there for me. I would also like to thank to my favorite person in the world, Can Fenerci.

Many thanks to Pourang Ezzatfar for his valuable help in the experimental part of this study. This research would not be possible without his valuable effort in the laboratory.

I would also like to thank my colleagues whom I worked with for two years. The warm atmosphere of room K7-Z01 has a great role in my success. It has been a pleasure to work with such smart and intellectual people. Especially, I am grateful to Başar Mutlu for his guidance about my subject.

Lastly, I want to thank the important people in my life. Friendships of Aras Şenlier, Barış Bingöl, Okan Özen, Tansu Güney, Ozan Akıncı, Taylan Özberk and Yaman Güray have been one of the few things which did not change during the last two years. Thank you guys for the great times.

TABLE OF CONTENTS

LIST OF TABLES

TABLES

LIST OF FIGURES

FIGURES

CHAPTER 1

INTRODUCTION

1.1. General

Reinforced concrete (RC) frames with unreinforced masonry (URM) infill walls are one of the most commonly used structural systems throughout the world. Such structural systems still preserve their popularity in seismic regions although they have suffered from severe earthquakes and resulted in major life and property loss in many Mediterranean and Latin American countries as well as Turkey, China, Iran and United States. In such systems, URM infill walls are generally considered as non-structural elements. They are used mainly as interior or exterior partitions in buildings to provide necessary space and functionality. Although URM infill walls serve as important architectural elements, they are also known to increase lateral strength and stiffness of the frame when the building is subjected to earthquakes (Fiorato et al. 1970; Brokken and Bertero 1983). The load resisting mechanism in a building is altered due to the presence of URM infill walls. Shortening of the natural vibration period as a result of the stiffness increase usually results in an increase in the earthquake forces on the structure. At high displacement demands, it is observed that the interaction of URM infill walls with their adjacent frame members may result in brittle shear failure of the neighboring columns, thereby limiting the deformability of the structure. Soft story mechanisms upon failure of the infill walls at a story may further pose threat for RC frame buildings. Recent earthquakes in Turkey and other earthquake prone countries drew attention to the importance of proper design and assessment of RC frames with URM infill walls. Presence of URM infill walls are usually neglected in the building design practice of many countries. This may result in unsafe design of boundary elements under the effect of lateral forces transferred from the infill walls. Isolation of masonry infill walls (Memari and Aliaari, 2004) can be used to accommodate large lateral frame deflections to prevent damage to boundary columns and infill walls. However, such methods are usually neither economical nor practical in the construction practice due to the heat transfer and fire performance requirements.

Seismically deficient buildings constitute a significant portion of the building stock in Turkey as well as other earthquake prone countries. Some of the common deficiencies in the Turkish building stock are low concrete strength, inadequate confinement or lap-splicing, insufficient member sizes, torsional or plan irregularities and having stronger beams compared to columns. Presence of such deficient buildings brings forth the requirement of accurate seismic assessment procedures for prevention of further life and property loss in case of earthquakes. Experimental testing has an important place in understanding the risk posed by earthquakes on deficient buildings. Experiments on seismically deficient frames also provide valuable data which can be used to verify the accuracy of the available seismic assessment methods on those buildings. In such buildings, the risk of shear failure on the boundary columns which may arise from the integral action of the infill walls and the frame structure can be even more critical compared to those observed in new buildings.

1.2. Problem Statement

Although vast amount of research has been done to investigate the seismic performance of URM infilled frames, the mechanics and modeling of the interaction between the frame elements and URM walls are not completely understood. The forces transferred to the boundary frame members due to the compression strut action needs further research. Numerical models which are capable of simulating the interaction behavior and the expected demand parameters can provide valuable information in this regard.

For the design of new structures, there are no regulations on the effect of infill walls or the boundary frame members in the Turkish Earthquake Code (TEC, 2007). URM infill walls are considered as non-structural components and they are not considered in the analysis during the course of the usual design procedure. This brings forth the requirement of evaluation of the current design codes by experimental and analytical research. Furthermore, the assessment methods in Chapter 7 of TEC (2007) do not provide any rules to consider the presence of infill walls. The shear design/assessment of the boundary frame members are conducted according to the capacity design principle which considers formation of plastic hinges at member ends. However, the distributed forces which will be transferred from the infill walls to the boundary frame members along the compression strut width are not considered. TEC has also no regulations concerning the risk of brittle shear failure of boundary frame members due to the infill wall-frame interaction. For the infill walls which has been retrofitted or reinforced with the techniques in the design code, the effect is claimed to be accounted by modeling the infill walls with strut models in the analyses. Considering these deficiencies in TEC, the performance of both code compliant and deficient RC frames should be examined. After careful research on the topic, necessary guidelines to consider frame-URM infill wall interaction should be adopted in TEC.

1.3. Literature Review

Over the past few decades, both the in-plane and out-of-plane interaction of infill walls with their bounding frames are experimentally investigated by many researchers. In-plane monotonic testing of the infill panels constitutes the majority of these studies. Literature on multi-story, multi-bay masonry infilled frame tests with hybrid simulation techniques or shake-table tests are rather limited. The experimental studies conducted on URM infilled frames and the observations of several researchers on both the behavior of infilled frames and the parameters affecting the behavior are briefed below.

Fiorato et al. (1970) conducted a comprehensive study on the beneficial effects of masonry infilled RC frames and tested 8 one-story one-bay, 13 five-story one-bay and 6 two-story three-bay 1/8-scale RC frames which had masonry infill walls on every bay. Brick masonry was used as the infill material and lateral monotonic and cyclic loading was applied on the specimens. They related the masonry infill wall material properties to the horizontal forces causing diagonal cracking and complete failure of the specimens. It was found that the presence of infill walls led to a considerable increase in the stiffness and the strength of the frames compared to non-infilled frames. It was also observed that the presence of infill walls in RC frames can introduce a reduced ductility and short-column failures.

Klingner and Bertero (1978) conducted quasi-static cyclic tests on two 1/3-scale specimens with clay brick and concrete block masonry infill walls which represented the lower three stories of an eleven-story prototype building. Frame members were designed for high ductility and infill reinforcement was used. Infill thickness was adjusted in such a way that the brittle shear failure of the columns would not occur. The failure was occurred at high displacement demands and the crushing of the infill wall followed by a soft story formation caused the failure for each specimen. They concluded that the infill walls in RC frames which were designed considering the frame-infill wall interaction were extremely beneficial in terms of stiffness and strength. The energy dissipation capacity and the ductility of the infilled frame were also better than that of the bare frame.

Mehrabi et al. (1994) carried out monotonic and cyclic experiments on fourteen 1/2-scale concrete block masonry infilled RC frames and investigated the effects of relative strength and stiffness of the infill walls in relation to their bounding frames, panel aspect ratio, magnitude and distribution of vertical loads, lateral loading history and presence of adjacent infilled bays. RC frames consisted of weak and strong frames designed as non-conforming and conforming according to the present seismic code regarding shear design. It was concluded that for the weak frames with strong infill panels, shear failure of the columns were occurred causing a brittle behavior for the entire frame structure. For the strong frames with relatively weak infill walls, flexural failure of the frame members was observed following the crushing of the infill wall.

Mosalam et al. (1998) tested a multi-story multi-bay concrete block masonry infilled steel frame with pseudo-dynamic (PsD) experimentation technique and conducted an

extensive study on the effect of openings in the infill walls. They observed that the infilled frame acted as an isolated frame in low displacement demands until the full contact between infill wall and the frame was achieved. It was observed that the first cracks occurred at the second story infill which had openings, however at the ultimate state, the damage in the first story infill wall was much more severe.

Fardis et al. (1999) conducted shake table experiments on a two-story, single-bay three-dimensional RC frame and studied the effects of plan irregularities caused by the non-uniform distribution of the masonry infill walls. They applied bi-directional loading on the frame and observed that despite the slenderness of the structure, out-of-plane failure of the infill wall did not occur even at high displacement demands. Another important finding was the displacement demands in case of the infilled frame were lower than that of the bare frame regardless of the period shortening caused by the increased stiffness.

Marjani and Ersoy (2002) investigated the behavior of brick infilled reinforced concrete frames under reversed cyclic loading and conducted experiments on six two-story one-bay frames. The researchers used both plastered and non-plastered infill walls to also investigate the effect of the plaster on stiffness and strength. They also tested six infill panels to determine the infill characteristics. By comparing the test results of the infilled and bare frame experiments, they concluded that the hollow clay tile infill walls increase both strength and stiffness significantly. The strength increase was about 240% for the non-plastered specimens and 300% for the plastered ones.

Hashemi and Mosalam (2007) conducted both shake table and PsD tests on a ¾ scale one story one bay R/C frame including the slab of the first floor and investigated also the out-of-plane behavior of the infill walls. It was found that the presence of the infill walls significantly increased strength and stiffness of the structure, caused shortening in the natural period and increased the damping coefficient. These effects had important influences on the force and displacement demands occurred on the structure. Results from experimental and analytical studies showed that the interaction between URM infill walls and their bounding frames were significant and neglecting this interaction could lead to both unsafe seismic risk evaluation and wrong identification of the most vulnerable elements in RC frames with URM infill walls.

Kurt et al. (2011) used PsD method for testing a seismically deficient ½ scale two story three bay RC frame and evaluated its seismic performance. The test frame had infill walls only at the middle bay and they found that the infill wall contributed to the strength about 65%. They also found that the assessment procedure provided by ASCE/SEI 41-06 (2006) gave considerably conservative results concerning the damage on the frame members.

Behavior and seismic strengthening of RC frames with brick infilled walls has also been the focus of many studies conducted in Middle East Technical University Structural Mechanics Laboratory over the past decade. Özcebe et al. (2003) conducted an intensive study about CFRP strengthening of seismically deficient and undamaged reinforced concrete frames and tested seven one-bay, two-story 1/3 scale RC frames. They con-

cluded that CFRP strengthening increases lateral strength significantly and decreases the ductility. Baran and Sevil (2010) tested three 1/3 scale one-story one-bay and 5 1/3 scale two-story one-bay RC frames with brick infill walls by changing axial load on columns, lap-splicing and mortar strength. They concluded that the strength increase was in the order of 6 times and the stiffness increase was about 20-30 times comparing with the bare frames. Akın (2011) conducted tests on eight 1/3 and four 1/2 scale two-story one-bay infilled RC frames with different aspect ratios. It was concluded that the initial stiffness and strength of the frames increased considerably. Contribution of infill walls in squat frames was larger compared to other frames due to more efficient strut formations. Okuyucu (2011) investigated the effect of aspect ratio of the frames in precast concrete panel strengthening technique. A total of fifteen 1/3 scale one-bay two-story RC frames were tested in the course of the study. She concluded that precast concrete panel application increased the lateral strength of the frames considerably.

Many researchers have focused on simulating the behavior of masonry infill walls inside building frames realizing the importance of their contribution to earthquake response. Various degrees of sophistication were employed in the infill models from macro models based on strut models which represent the behavior of the URM infill wall with truss elements connected to the frame elements to micro models which are more complicated continuum finite element models based on smeared or discrete cracking approaches. Although macro modeling approach still preserves its popularity due to its ease of application and implementation in practice, more complicated models are necessary for research purposes and more accurate estimations of local failure modes and forces transferred to boundary elements.

Klingner and Bertero (1978) employed diagonal strut elements for representing the URM infill wall in their finite element method. They concluded that diagonal strut modeling provided good agreement with the experimental results in the global sense.

El-Dakhakhni et al. (2003) also adopted the macro modeling approach; however they stated that the real strut mechanism is composed of a portion of the infill wall, forming stressed regions at the two loaded corners rather than a simple truss connecting two corners of the bounding frame. They proposed a model composed of three parallel struts in each direction.

Hashemi and Mosalam (2007) modeled the URM infill wall as a continuum with smeared crack finite elements and used nonlinear frame elements to model the bounding frame. They used interface elements for the frame-infill interfaces. The results obtained from the analyses were in almost perfect agreement with the shake table and PsD experiments. They also proposed a three-dimensional strut and tie model composed of eight compression struts and a tension tie to simulate both the in-plane and out-of-plane behavior of the infill wall.

More recently, Stavridis and Shing (2010) employed the micro modeling technique and combined the smeared and discrete crack approaches to simulate the shear failures in RC

boundary columns. They were able to capture the global load-deformation response and the inclined cracking in the boundary columns with their approach.

1.4. Guidelines on the Design and Assessment of RC Frames with URM Infill Walls

Eurocode 8 (2004) which is the current structural design code for earthquake resistance for European countries provides regulations for RC frames with URM infill walls. In Eurocode 8, the beneficial effects of the infill walls on seismic performance are not taken into account. Instead, the designers are warned against the adverse effects of infill walls such as possible soft story formations, plan irregularities and shear failure in boundary columns. For preventing soft story failures, the columns of a story where the infill walls are reduced relative to the overlying story, should be designed to remain in its elastic range until the infill walls in the overlying story loses their capacity. To overcome the torsional response arising from the asymmetric distribution of infill walls, Eurocode 8 doubles accidental eccentricity to be used in the analysis. The effect of the forces which will be transferred from the infill wall to the boundary columns are also taken into account and the boundary columns should be designed for the smaller of the two shear forces which will be computed from:

- The horizontal component of the infill strut force which is equal to the horizontal shear strength of the panel
- The shear force calculated considering the short column formation following corner crushing of the infill along its strut width

The illustration of the expected shear force transferred and the strut width is given in Figure 1.1. Eurocode 8 also has taken measures for the possible seismically induced soft-story mechanism in the ground floors due to the particular vulnerability of the infill walls. The entire length of the first story columns are considered as the critical length and confined.

ASCE/SEI 41-06 is the seismic assessment code provided by the American Society of Civil Engineers which replaced FEMA 356 (Pre-standard and Commentary for the Seismic Rehabilitation of Buildings, 2000) in 2006. Shortly after, an update named ASCE/SEI 41 Supplement-1 was released based on the research that has been carried on since the release of the first document. ASCE/SEI 41-06 provides guidelines for assessment and rehabilitation of RC frames with URM infill walls. For the isolated frame members, the assessment is made based on plastic rotation in the plastic hinge regions, whereas it is based on total column average strain in case of boundary columns. Plastic rotation limits provided for the isolated column members are given in

Table 1.1. In the table, P is the axial load on the member, A_g is the gross area of the column section and f_c' is the concrete strength where ρ stands for the transverse rein-

forcement ratio of the section and V stands for the shear demand on the column which will be calculated from plastic hinge formation at both ends of the members. Section dimensions are represented by b_w and d. The frame members adjacent to infill walls are considered as axial load-carrying members and generalized displacement will be taken as axial deformation of member rather than rotation in plastic hinge region in modeling of those members. Strain limits are given in Table 1.2. ASCE/SEI 41-06 also provides methods to estimate the forces which are transferred from the infill walls to the adjacent beams and columns. Similar to Eurocode 8, the estimation of the forces transferred is based on the horizontal component of the strut force originating from the full shear strength development in the infill wall and the short column formation resulting from corner crushing, however it is not limited to columns. Then the shear strength of boundary columns and beams should be checked against those forces. If the shear strength of the columns and beams are found as insufficient, the members need to be strengthened according to ASCE/SEI 41-06. For the assessment of the infill walls, a drift based procedure is recommended by the document. Performance limits are provided in terms of inter-story drift ratio of the story and depends on the aspect ratio and frame strength to infill wall strength ratio. The drift limits are given in

Table 1.3. Here, V_{fre} and V_{ine} are lateral frame and infill wall strengths respectively where L_{inf}/h_{inf} is the length to height aspect ratio of the infill panel.

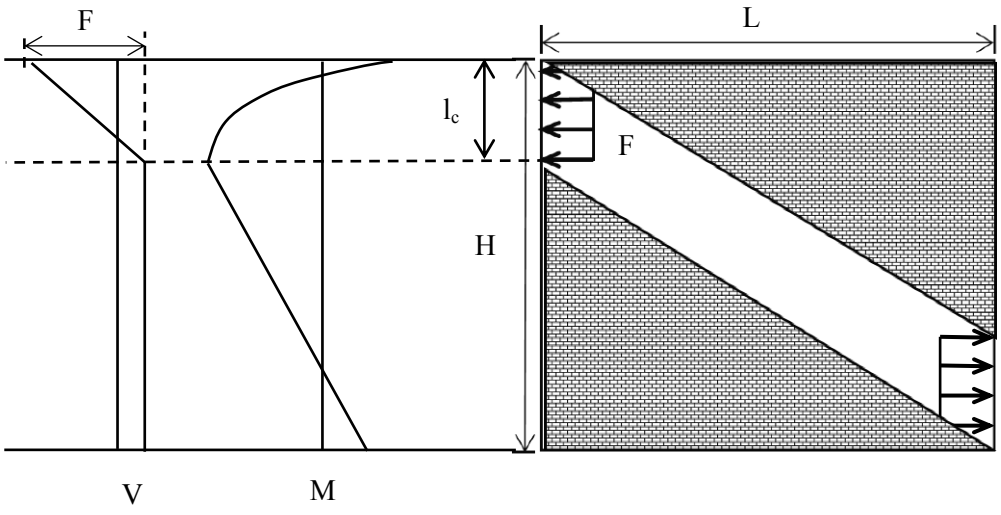

Figure 1.1: Expected Shear Force Transferred from the Infill Wall According to Eurocode 8 (2004)

Table 1.1: Numerical Acceptance Criteria for RC Columns in ASCE/SEI 41-06

Condition i.			**Acceptance Criteria**		
			Plastic Rotations Angle, radians		
			Performance Level		
$\frac{P}{A_g f_c'}$	$\rho = \frac{A_v}{b_w s}$		IO	LS	CP
≤ 0.1	≥ 0.006		0.005	0.026	0.035
≥ 0.6	≥ 0.006		0.003	0.008	0.009
≤ 0.1	= 0.002		0.005	0.02	0.027
≥ 0.6	= 0.002		0.002	0.003	0.004
Condition ii.			**Acceptance Criteria**		
			Plastic Rotations Angle, radians		
			Performance Level		
$\frac{P}{A_g f_c'}$	$\rho = \frac{A_v}{b_w s}$	$\frac{V}{b_w d\sqrt{f_c'}}$	IO	LS	CP
≤ 0.1	≥ 0.006	≤ 3	0.005	0.024	0.032
≤ 0.1	≥ 0.006	≥ 6	0.005	0.019	0.025
≥ 0.6	≥ 0.006	≤ 3	0.003	0.008	0.009
≥ 0.6	≥ 0.006	≥ 6	0.003	0.006	0.007
≤ 0.1	≤ 0.0005	≤ 3	0.005	0.009	0.01
≤ 0.1	≤ 0.0005	≥ 6	0.004	0.005	0.005
≥ 0.6	≤ 0.0005	≤ 3	0.002	0.003	0.003
≥ 0.6	≤ 0.0005	≥ 6	0	0	0

IO: Immediate Occupancy, LS: Life Safety, CP: Collapse Prevention

Table 1.2: Numerical Acceptance Criteria for Infilled RC Columns in ASCE/SEI 41-06

	Acceptance Criteria		
	Total Strain		
	Performance Level		
Conditions	IO	LS	CP
i. Columns modeled as compression chords			
Columns confined along entire length	0.003	0.015	0.02
All other cases	0.002	0.002	0.003
ii. Columns modeled as tension chords			
Columns with well-confined splices, or no splices	0.01	0.03	0.04
All other cases	See the document		

IO: Immediate Occupancy, LS: Life Safety, CP: Collapse Prevention

Table 1.3: Numerical Acceptance Criteria for Masonry Infill Walls in ASCE/SEI 41-06

		Acceptance Criteria
$\beta = V_{fre} / V_{ine}$	**L_{inf}/h_{inf}**	**LS (%)**
$\beta < 0.7$	0.5	0.4
	1	0.3
	2	0.2
$0.7 \leq \beta < 1.3$	0.5	0.8
	1	0.6
	2	0.4
$\beta \geq 1.3$	0.5	1.1
	1	0.9
	2	0.7

LS: Life Safety

1.5. Objective and Scope

The uncertainties concerning the performance of design and assessment guidelines on predicting the risk of shear failures of boundary columns due to the frame-infill wall interaction renders the need of further experimental and analytical research on the subject. In this respect, the performance of the two test specimens which was constructed and tested at METU Structural Mechanics Laboratory was studied. The test specimens were among many specimens tested in the scope of the comprehensive research project named "Investigation and Development of Performance Based Assessment and Strengthening Techniques for New Generation Seismic Codes" funded by The Scientific and Technological Research Council of Turkey (TÜBİTAK KAMAG 1007, 108G034, 2010-2013). The PsD experiments were conducted by a research team consisted of research and project assistants at METU. The test specimens used in this study were prepared by laboratory technicians under the supervision of Pourang Ezzatfar, Mehmet Engin Ayatar and faculty members. Testing was conducted under the supervision of faculty members with the help from Salim Azak and aforementioned Ph.D candıdates. The experiemntal data produced from testing was used in this thesis solely to compare the results with simulations and calibrate finite element models. Further information on the tests and their comaprsions with other specimens will be presented by Poureng Ezzatfar in his Ph.D thesis. Two specimens among thirteen specimens which were tested in the course of the project was studied here. The specimens which were named as Specimen 2 and Specimen 6 in the project will be referred as Specimen 1 and 2 in this study, respectively. The first of the test frames which will be addressed as Specimen 1 in this thesis was designed according to the Turkish Earthquake Code (TEC, 2007) which includes all the principles of modern earthquake resistant design excluding the effect of the infill

walls. Specimen 2 was a seismically deficient frame which was intentionally designed inadequately according to the current seismic code to represent the deficiencies present in the existing buildings in Turkey. Pseudo dynamic testing was conducted under three levels of ground motion on both test specimens.

The main objective of this study was to investigate the hazard on the boundary columns posed by the frame-infill wall interaction in RC frames with URM infill walls. In this respect, post-processing of the experimental data from PsD experiments on the two specimens were done. A nonlinear continuum finite element model was developed and the ability of the model to estimate the local and global engineering demand parameters was investigated. Afterwards, the results of the nonlinear analysis were employed to deduce the force distributions on the boundary columns which could not be obtained from the experiments. Finally, the accuracy of the ASCE/SEI-41-06 guidelines for the assessment of infill walls and boundary columns in estimating the observed damage was critically evaluated.

In Chapter 2, the experimental and analytical study concerning the code compliant frame (Specimen 1) is addressed. Here, the test setup, instrumentation and the testing procedure is explained briefly and experimental results are presented and interpreted. Numerical modeling approach is given and validated. After that, dynamic analysis results were given along with the experimental results and forces occurred on the boundary columns are further studied. The experimental and analytical results of the deficient frame (Specimen 2) are presented in Chapter 3. Seismic assessment of the two specimens along with nine experiments conducted by Mehrabi (1994) was made according to ASCE/SEI 41-06 guidelines and interpretation of the results was given along with the assessment results.

CHAPTER 2

CODE COMPLIANT FRAME

In this chapter, the behavior of a code compliant frame and its interaction with its infill walls are examined in light of both experimental and numerical simulation results. The properties of the code compliant test specimen are presented. The testing methodology, test setup and the instrumentation are explained briefly. Results of the PsD experiment under three levels of ground motion are presented and interpreted. The presented results include inter-story drifts and force deformation responses of each story. The formulation used for obtaining the identification of dynamic parameters is given and the identified natural vibration period and damping ratio histories are also presented.

Numerical modeling approach is explained briefly and validated with experiments from Mehrabi (1994). Dynamic analysis results under three levels of ground motion are presented and the accuracy of the model to simulate both global and local demand parameters is investigated. Here, results of the dynamic analysis are given together with the experimental results. These results include force deformation relationships and inter-story drift ratios at each story, strain and rotation demands at the plastic hinge regions of column members and moment-curvature relationships of exterior columns. In order to further elaborate on the interaction behavior and forces occurring at the boundary columns, shear diagrams of the first story columns, the corresponding strut width and distributed loading on the boundary columns are obtained from the analysis results and presented in this chapter along with the ASCE/SEI 41-06 recommendations.

2.1. Properties of Specimen 1

The ½ scaled three story-three bay reinforced concrete frame with masonry infill walls at its central bay was selected from a typical interior frame of an RC prototype building (Figure 2.1.a). The building was designed according to the TEC (2007) provisions. Gravity loads were applied on the beams with flanged sections to represent the dead and live loads by steel blocks (Figure 2.1.a). Applied gravity loads were 94 kN for the first two stories and 88 kN for the third story. Columns had dimensions of 150 mm × 200 mm with a longitudinal reinforcement ratio of 2.3% (8ϕ10 mm as shown in Figure 2.1.b). Beams had flanged sections with a bottom width of 150 mm and the height of the section including the flange was 175 mm. Flange thickness was 60 mm and flange width was 500 mm. Details of the beam section and the reinforcement used are shown in Figure 2.1.b. 4 mm diameter stirrups were used as transverse reinforcement along with intermediate ties and end zones at the end of both beams and columns were properly confined (Figure 2.1.b). Infill walls were constructed according to the common construction practice by using hollow clay bricks which had dimensions of 95 mm × 100 mm × 190 mm (Figure 2.1.b). The holes of the hollow clay brick units were placed parallel to the vertical direction. Thickness of the applied plaster on the infill wall surfaces on both sides was approximately 10 mm. Uniaxial compressive tests on concrete cylinder specimens revealed an average compressive strength of 19.6 MPa. The average uniaxial compressive strength of mortar and plaster were 4.2 MPa and the hollow clay brick units had a uniaxial compressive strength of 8.5 MPa. 8 mm deformed bars were used as longitudinal reinforcement with a yield strength of 480 MPa and an ultimate strength of 640 MPa. 10 mm deformed bars, which were used as longitudinal reinforcement, had a yield strength of 480 MPa and an ultimate strength of 750 MPa. 4 mm bars used were plain bars with a yield strength of 240 MPa and ultimate strength of 340 MPa.

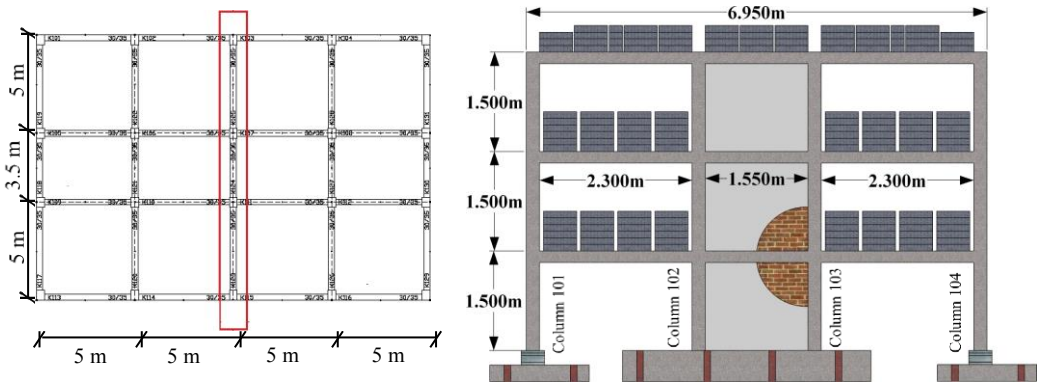

a) Prototype Structure and Test Frame

Figure 2.1: Details of the Specimen 1 (cont'd)

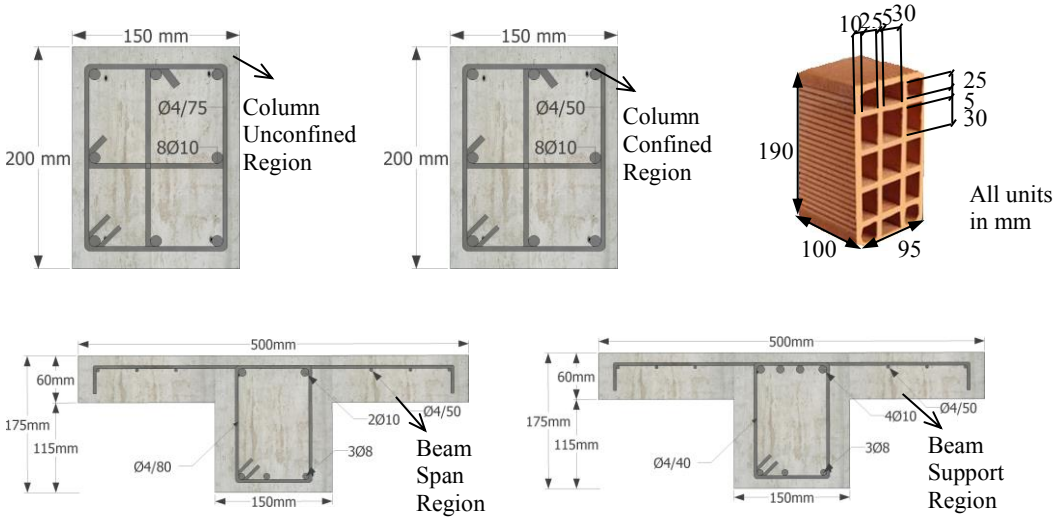

b) Section Properties

Figure 2.1: Details of the Specimen 1 (cont'd)

2.2. Instrumentation and Testing

Instrumentation consisted of Linear Variable Differential Transformers (LVDTs) which were placed at each story level and at the member ends, load cells at story levels, electrical dial gages placed at the infill wall diagonals and force transducers at the bottom of the exterior columns. LVDTs were placed at each story level and the member ends of the first two story columns and beams to measure the story deformations, member end rotations and curvatures. For the calculation of member end rotations and curvatures, measurements taken from two LVDTs placed on the opposite faces of the beam in the bending direction. Base moments, shear and axial forces were obtained by the three component force transducers attached at the bottom of the exterior columns (Canbay et al. 2004). Dial gages were used to measure the strains on the infill diagonals at each story. Story shears were obtained by the use of load cells at each floor level. Details of the instrumentation and LVDTs used in the calculations in the course of this study are presented in Figure 2.2.

For the testing of the frame, pseudo-dynamic (PsD) testing technique, which is a hybrid simulation and testing method, was used. PsD method was proposed as an alternative method to shake table testing by Takanashi et al. (1975) and was found to be advantageous in many aspects. It allows large scale testing and observation of the damage propagation due to the slow application of the earthquake loading. In PsD testing method, part of the structure namely the damping and mass properties are defined numerically and the rest of the structure is physically tested along with the numerical integration of the equation of motion at each step. The restoring forces are measured from the experi-

ment and used to numerically solve the equation of motion for the corresponding displacements. Obtained displacements are then imposed to the structure for the next step. Use of explicit methods for numerical integration which rules out the need for iterations was proved to be valid in pseudo-dynamic experimentation (Mahin and Shing, 1984). An illustration of the PsD test loop is presented in Figure 2.3.

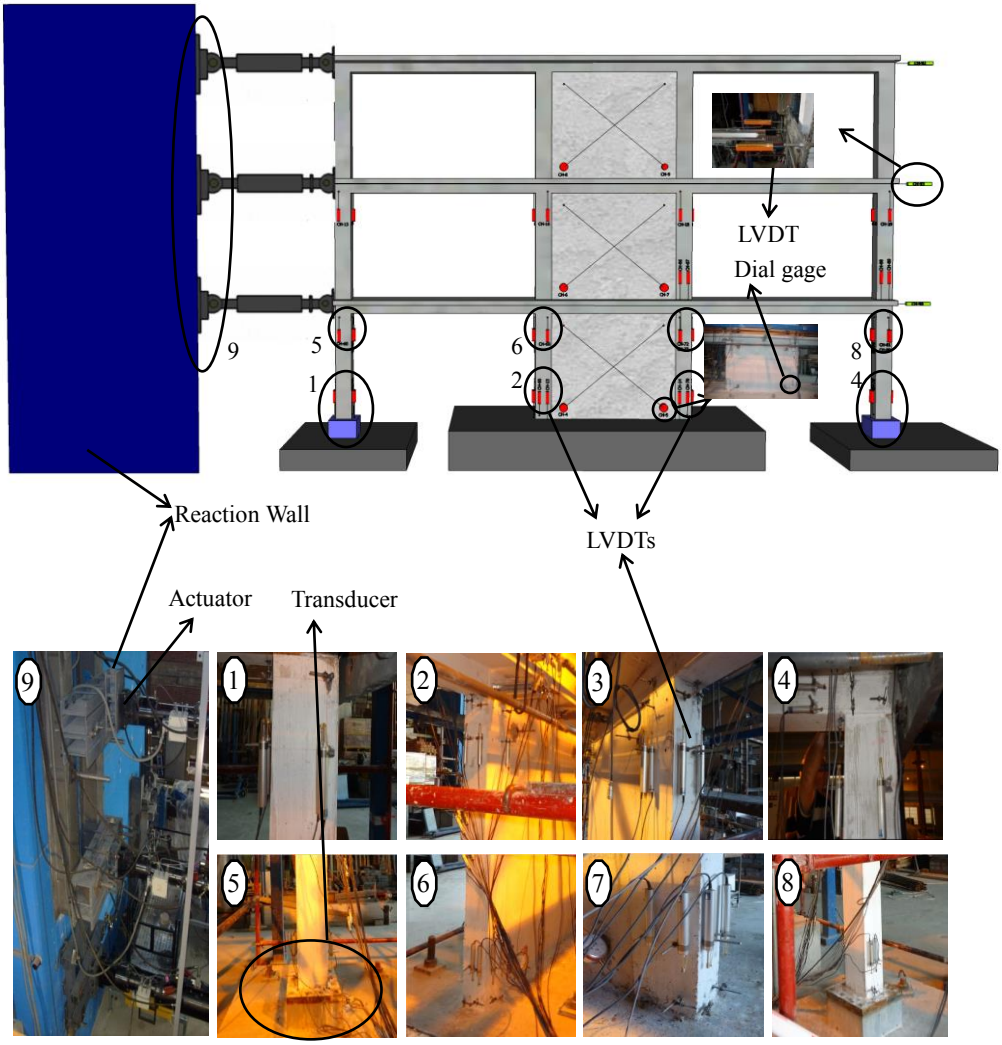

Figure 2.2: Test Setup and Instrumentation

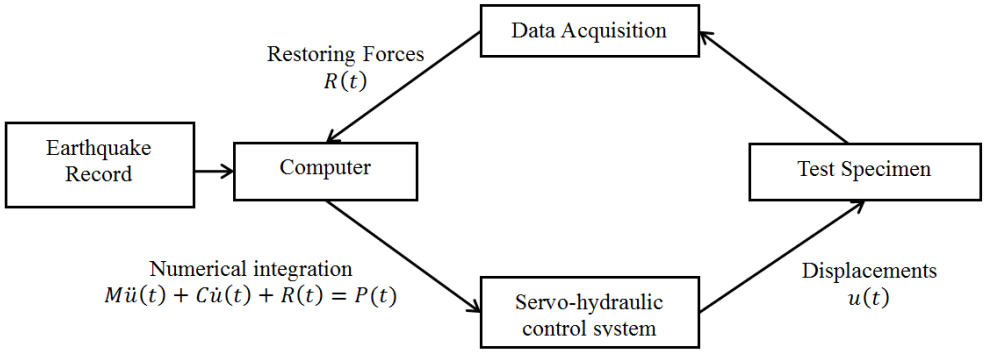

Figure 2.3: Pseudo-dynamic Testing Loop

The three degree-of-freedom system was tested using the continuous PsD method (Molina et al. 1999). Using the ground acceleration record, the equation of motion for the structure was solved numerically with an explicit time integration scheme and the obtained displacement demands were applied to the structure with the help of the hydraulic actuators. Mass matrix used was diagonal and consistent with the actual story masses (m_1 = 11426 kg, m_2 = 11426 kg, m_3 = 7925 kg) and zero damping was defined to the system. Three synthetic ground acceleration records were generated and scaled to match the site specific spectra of Düzce region. D1 and D2 ground motions represent 50% and 10% probability of being exceeded in 50 years for Z1 type of soil respectively, whereas D4 ground motion represents 10% probability of being exceeded in 50 years for Z3 type of soil. Original ground motions were compressed within the time domain by the factor of $1/\sqrt{2}$, compatible with the similitude law. The ground motions used and the corresponding earthquake spectra are shown in Figure 2.4.

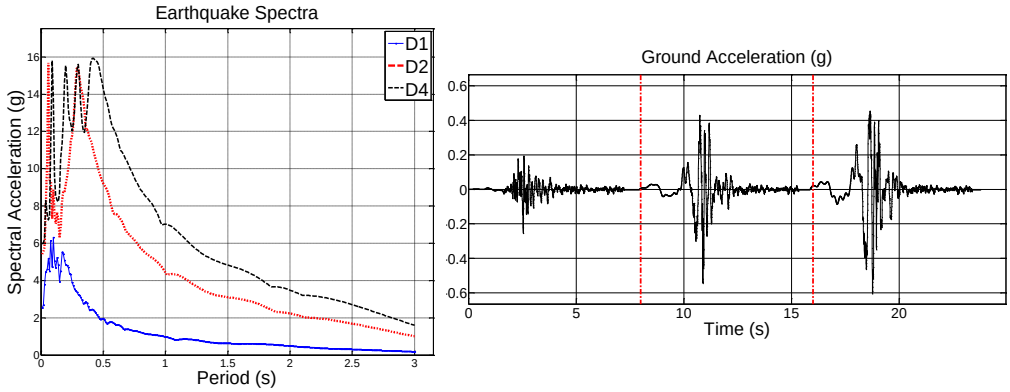

Figure 2.4: Ground Motions Used in Experiments

2.3. Experimental Results

The inter-story drift ratios of the three stories are presented along with the damage patterns, which were observed during the peak deformation instants of the experiment are given in Figure 2.5. Force-deformation relationships of each story in the form of story shear versus inter-story drift ratio are given in Figure 2.6. From the force-displacement envelopes, it is observed that the overall load carrying capacity of the test frame did not decrease significantly even at the end of the experiment. However, sudden drops in strength values were observed during D2 and D4 earthquakes which coincide with the cracking of the first and second story infill walls.

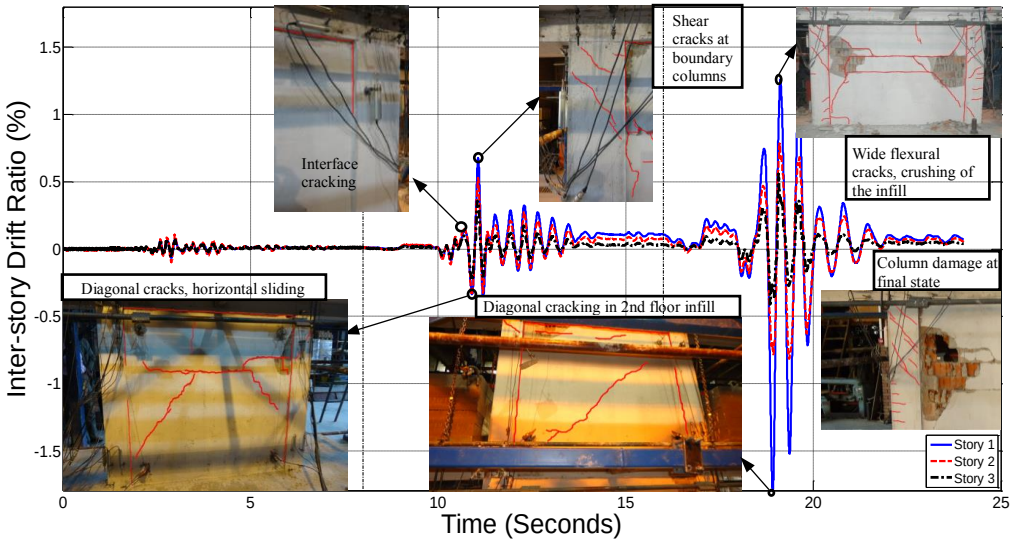

Figure 2.5: Inter-Story Drift Ratio Response along with Damage Patterns for Specimen1

For the D1 earthquake, the test frame did not show any nonlinear behavior and exhibited very small displacement demands. D2 earthquake resulted in interface cracks at the frame- infill wall boundaries. Horizontal sliding cracks at the infill and cracks at boundary columns due to frame- infill wall interaction were also observed. Maximum inter-story drift ratio of the first story at the end of D2 earthquake was about 0.7% at a roof displacement of 28 mm. D4 earthquake caused significant damage on the test frame, resulting in widening of the existing diagonal cracks in the first story infill wall, which resulted the test frame to experience large first story drifts. Corner crushing of the first

story infill wall and flexural and shear cracks at columns were also observed. In the second story, interface cracks at the frame-infill wall boundary and a diagonal crack at the URM infill wall were observed. For this ground motion, maximum inter-story drift ratio of the first floor was about 2.0% resulting in 43 mm roof displacement. Maximum base shear demand measured during experiment was 200 kN. Base shear versus roof displacement responses for the D1, D2 and D4 ground motions are presented in Figure 2.6. Diagonal wall strains measured in the first story infill wall diagonals are given in Figure 2.7. Results concerning the local demand parameters such as member-end rotations and curvatures are presented and discussed in the numerical simulations part.

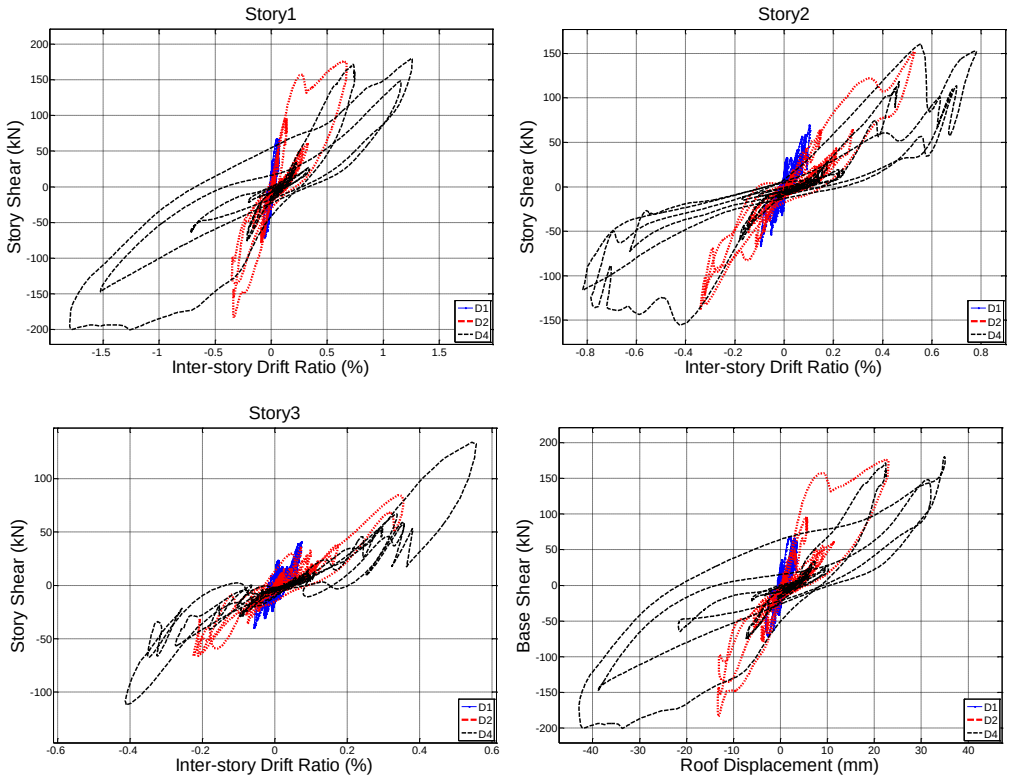

Figure 2.6: Force - Deformation Response for Specimen 1

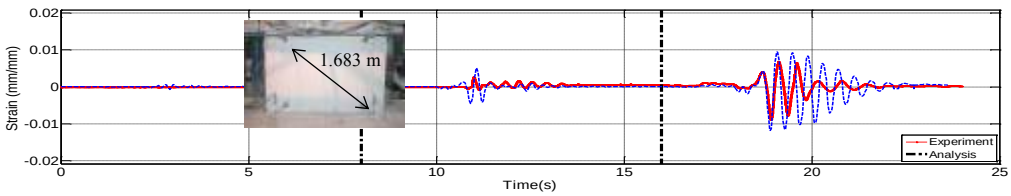

Figure 2.7: Diagonal Wall Strain Response for the First Story for Specimen 1

2.4. Identification of Dynamic Parameters

Identification of the time dependent vibration periods and damping ratios of the test frame is obtained using the procedure proposed by Molina et al. (1999) which uses results of the PsD method for the identification of eigenmodes of the test frame. In this model, the measured restoring forces $\boldsymbol{r}(n)$, applied displacements $\boldsymbol{u}(n)$ and the velocities $\boldsymbol{v}(n)$ are considered to be related as:

$$[\boldsymbol{u}^T(n) \quad \boldsymbol{v}^T(n) \quad \mathbf{1}] \cdot \begin{bmatrix} \boldsymbol{K}^T \\ \boldsymbol{C}^T \\ \boldsymbol{o}^T \end{bmatrix} = \boldsymbol{r}^T(n) \tag{2.1}$$

where $\boldsymbol{K}$ and $\boldsymbol{C}$ are the secant stiffness and viscous damping matrices and $\boldsymbol{o}$ is constant force offset term. It should be noted that the solution is only possible with using a number of time steps. Obtaining a least squares solution for $\boldsymbol{K}$ and $\boldsymbol{C}$, eigen frequencies and mode shapes for the problem can be obtained by solving the generalized eigenvalue problem given by Maia and Silva (1997):

$$s\begin{bmatrix} \boldsymbol{C} & \boldsymbol{M} \\ \boldsymbol{M} & \mathbf{0} \end{bmatrix}\boldsymbol{v} + \begin{bmatrix} \boldsymbol{K} & \mathbf{0} \\ \mathbf{0} & -\boldsymbol{M} \end{bmatrix}\boldsymbol{v}=0 \tag{2.2}$$

$$s_i, s_i^* = w_i\left(\zeta_i \pm j\sqrt{1-\zeta_i^2}\right) \tag{2.3}$$

where

$$j^2 = -1$$

and **M** is the theoretical mass matrix which is used in the PsD experiment. Natural frequency w_i and the equivalent viscous damping ratio ζ_i at the i^{th} mode can then be obtained using Equation 2.3. Identified first mode period and damping ratios are shown in Figure 2.8. It is observed that the first mode period of the test frame was about 0.17 sec at the beginning of the test and didn't change significantly until the end of D1 ground motion. The period elongated to about 0.3 seconds at the end of the D2 ground motion. At the end of the experiment, the fundamental period was about 0.53 seconds. This elongation in the period can easily be attributed to both cracking of the URM infill wall and flexural cracking of frame members which reduce the initial stiffness of the structure. It is observed that the damping ratio was about 5% at the beginning of the experiment and was about 20% during the rest of the experiment, with several peaks. It is also noted that the locations of significant oscillations in both graphs coincide and related with the loss of numerical stability of the method during time intervals of highly inelastic actions.

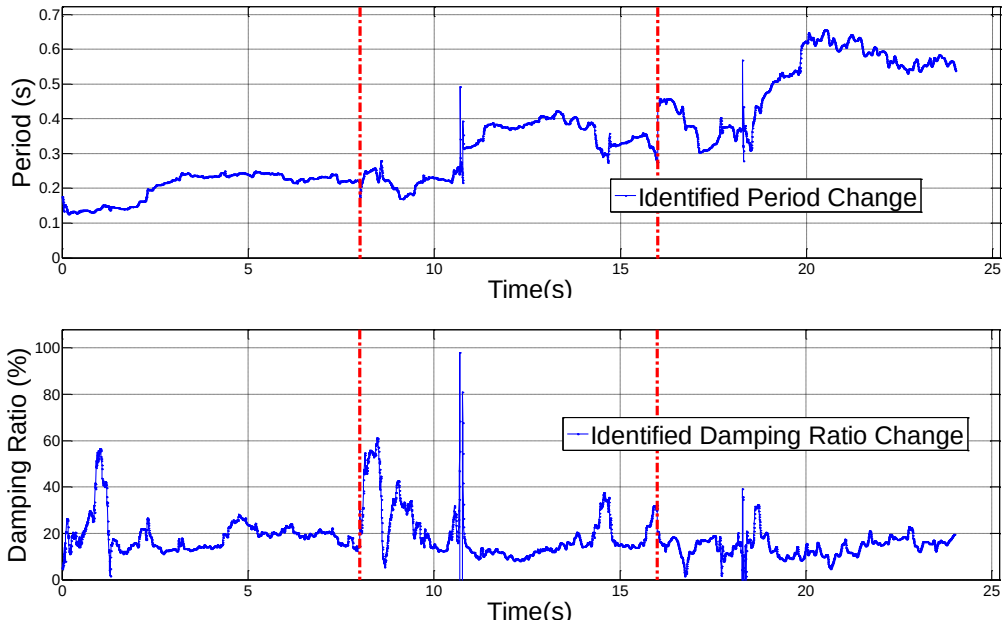

Figure 2.8: Identified Period and Damping Ratio for Specimen 1

2.5. Numerical Modeling

The test frame was modeled as a continuum in plane stress by using finite element method employing DIANA (2008). The reinforced concrete frame was modeled with 8-node quadrilateral elements which were based on quadratic interpolation and integrated numerically by a 2 × 2 Gauss integration method. Total strain rotating crack model was used to model the nonlinear behavior of both reinforced concrete and masonry. Material model describes both the compressive and tensile behavior by stress–strain relationships in the principle directions. Concrete behavior was modeled as a linear elastic-brittle material in tension and elastic perfectly plastic in compression. For the lateral confinement, model proposed by Selby and Vecchio (1993) was used. Since the frame was modeled as a plane stress problem, the effect of the confining pressure in the third dimension cannot be incorporated directly. Therefore, the use of a simplified and stable uniaxial stress-strain model was preferred owing to the absence of concrete crushing observation in the tests. For the reinforcing steel, embedded reinforcement approach (DIANA 2008) was used. Reinforcing bars were modeled at their exact geometric locations in the finite element mesh. Perfect bond was assumed between concrete and steel. For steel, Von-Mises yield criterion was used with a bilinear stress-strain curve in uniaxial tension. The frame-infill wall interfaces were modeled using 6-node interface elements with a Coulomb Friction criterion. Linear normal and tangential stiffnesses of interfaces were assumed to be equal to each other. Cohesion and friction hardening regions were ignored and a non-associated flow rule was used with a gap criterion defined

with very low tensile strength. This model assumed that a gap forms if the tensile traction strength is exceeded. Smeared crack approach was also employed for the modeling of the URM infill wall using 8-node quadrilateral iso-parametric plane-stress finite elements. Material behavior was considered as linear elastic and brittle in tension, parabolic in compression with the conventional formulation of the total strain rotating crack approach. For the lateral cracking, model proposed by Vecchio and Collins (1993) was used. The gravity loading which was applied by steel blocks was simulated as distributed loads on beams. Material properties regarding steel and concrete are taken directly from material test. Story masses were defined consistent with the mass matrix as used in the PsD system and lumped at the nodes. The final finite element mesh composed of 4917 plane stress elements and 342 interface elements. Nonlinear time history analysis of the finite element mesh took about 8 hours using three consecutive ground motions. All the material properties used in the simulations are given in Table 2.1 and a summary of the modeling strategy is presented in Figure 2.9.

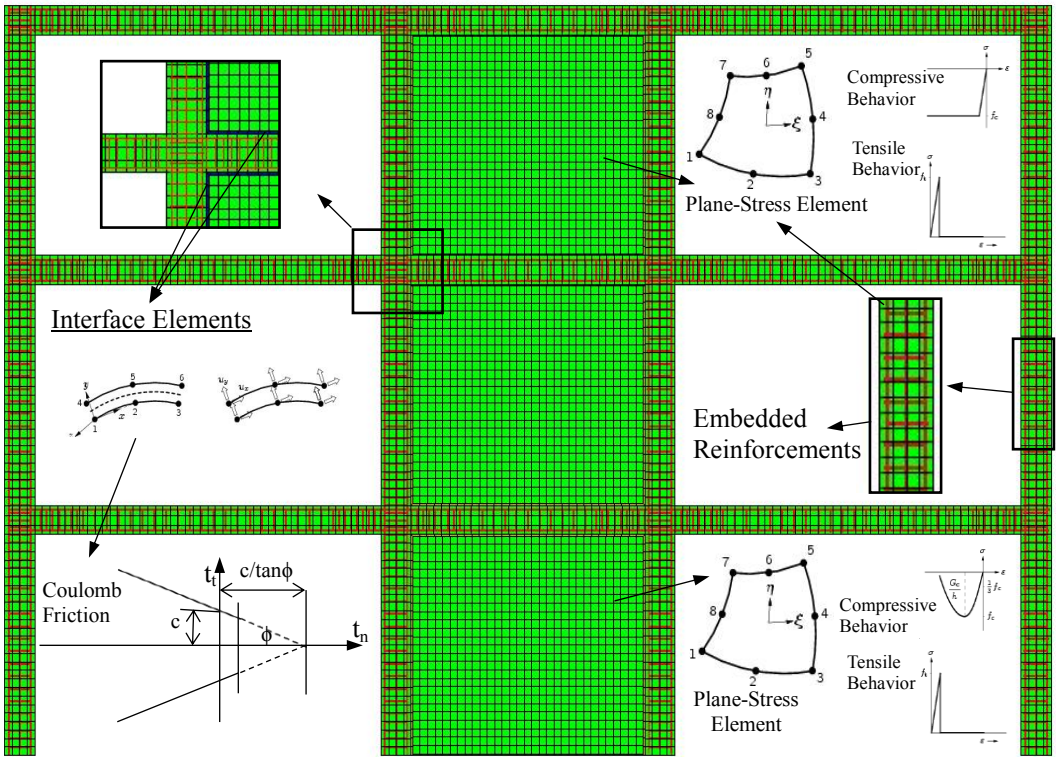

Figure 2.9: Modeling Strategy

Table 2.1: Material Properties Used in Numerical Simulations of Specimen 1

Wall Medium		**Mortar (Interfaces)**		
Elastic Modulus E_c (MPa)	850	Normal Stiffness K_{nn} (N/m^3)		8.5×10^{11}
Compressive Strength f'_c (MPa)	5	Tangential Stiffness K_{tt} (N/m^3)		8.5×10^{11}
Tensile Strength f_{ct} (MPa)	0.25	Cohesion c (MPa)		0.5
Fracture Energy (N.m)	196777	Friction Angle (tanφ)		0.5
Concrete		**Reinforcing Steel**		
		Reinforcing Bar	**Yield Strength (MPa)**	**Ultimate Strength (MPa)**
Elastic Modulus E_c (MPa)	21029	4 mm plain bars	240	340
Compressive Strength f'_c (MPa)	19.6	8 mm deformed bars	450	640
Tensile Strength f_{ct} (MPa)	1.55	10 mm deformed bars	450	720

2.6. Validation of the Proposed Model

2.6.1. Monotonic Analyses

The capability of the proposed FE model to simulate the highly nonlinear behavior of the frame-infill wall interaction and the resulting failure modes were investigated using experiments conducted by Mehrabi et al. (1994). 10 single-story single-bay RC frames with different infill wall and frame characteristics were tested monotonically or cyclically at University of Colorado at Boulder, a summary of the experimental study and material properties are given in Table 2.2. Section details of both weak and strong frames are given in Figure 2.10. The modeling strategy described earlier was employed here without any alterations to validate the model. Here, elastic stiffness properties of interfaces were obtained from joint direct shear tests which were conducted on mortar specimens. Results of the cyclic joint direct shear tests are given in Figure 2.11. The performance of the model of simulating the force-deformation relationships (pushover curves) and damage propagation in the structure is evaluated.

Table 2.2: Characteristics and Material Properties of the Frame Specimens

Specimen	Frame	Panel Height (m)	Panel aspect ratio (h/l)	Brick Type	Infill Thick. (mm)	E_c (MPa)	f_c (MPa)	E_m (MPa)	f_{cm}* (MPa)	Loading
Sp1	weak	1.35	0.67	-	-	21926	30.9	-	-	mon.
Sp2	weak	1.35	0.67	hol.	45	21926	30.9	3150.6	9.7	mon.
Sp3	weak	1.35	0.67	solid	90	21926	30.9	9520.6	15.1	mon.
Sp4	weak	1.35	0.67	hol.	45	17237	26.8	4598.8	10.6	cyc.
Sp5	weak	1.35	0.67	solid	90	18064	20.9	8949.4	13.9	cyc.
Sp6	strong	1.35	0.67	hol.	45	19857	25.9	4198.9	10.1	cyc.
Sp7	strong	1.35	0.67	solid	90	18616	33.4	9073.5	13.6	cyc.
Sp8	weak	1.35	0.67	hol.	45	17237	26.8	5102.1	9.5	mon.
Sp9	weak	1.35	0.67	solid	90	17237	26.8	8239.2	14.2	mon.
Sp10	weak	1.35	0.48	hol.	45	201334	26.9	3943.8	10.6	cyc.

*fcm was obtained from triplet tests on masonry assemblages

hol.: hollow, mon.: monotonic, cyc.:cyclic

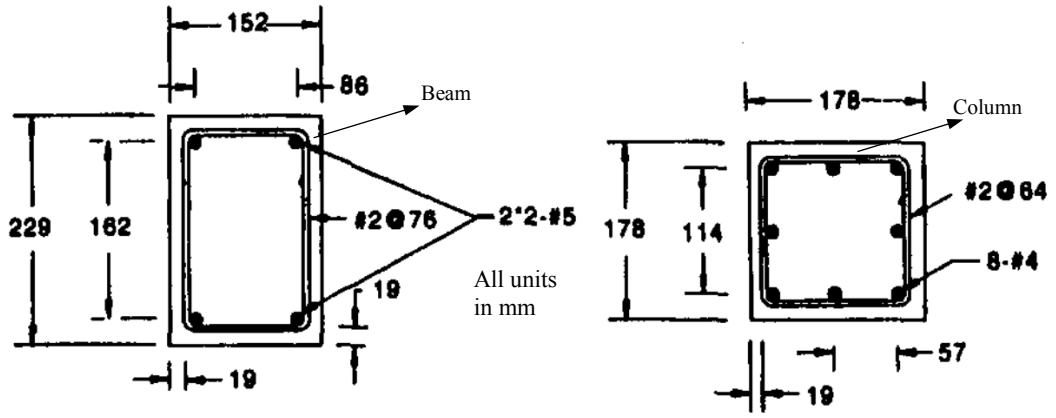

a) Weak Frame

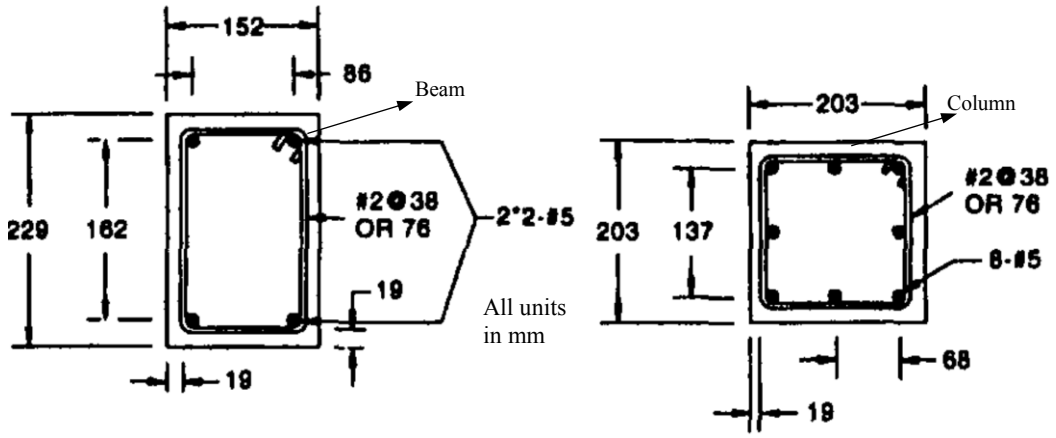

b) Strong Frame

Figure 2.10: Section Details of Test Specimens (Mehrabi, 1994)

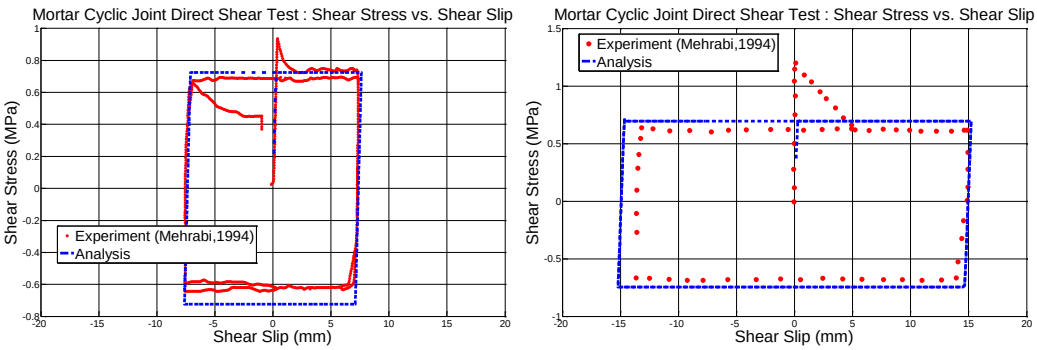

a) Hollow Brick *b) Solid Brick*

Figure 2.11: Results of Cyclic Joint Direct Shear Tests (Mehrabi, 1994)

Inelastic pushover analyses were carried out for each test frame. The finite element mesh used in the simulations is presented in Figure 2.12. The results of the analyses are presented along with the experimental results. Errors of stiffness and load carrying capacity were also calculated (Figure 2.13). Both experimental and analytical stiffness values were obtained by extending a straight line from origin to the point of 75% of the ultimate load carrying capacity. From the load-displacement envelopes and error quantities, it is observed that there was a reasonable agreement between the experimental and numerical simulation results in terms of load carrying capacity and initial stiffness.

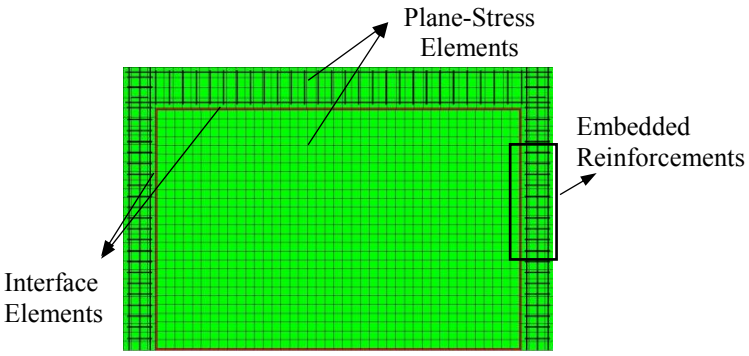

Figure 2.12: FE Mesh used in the Simulations

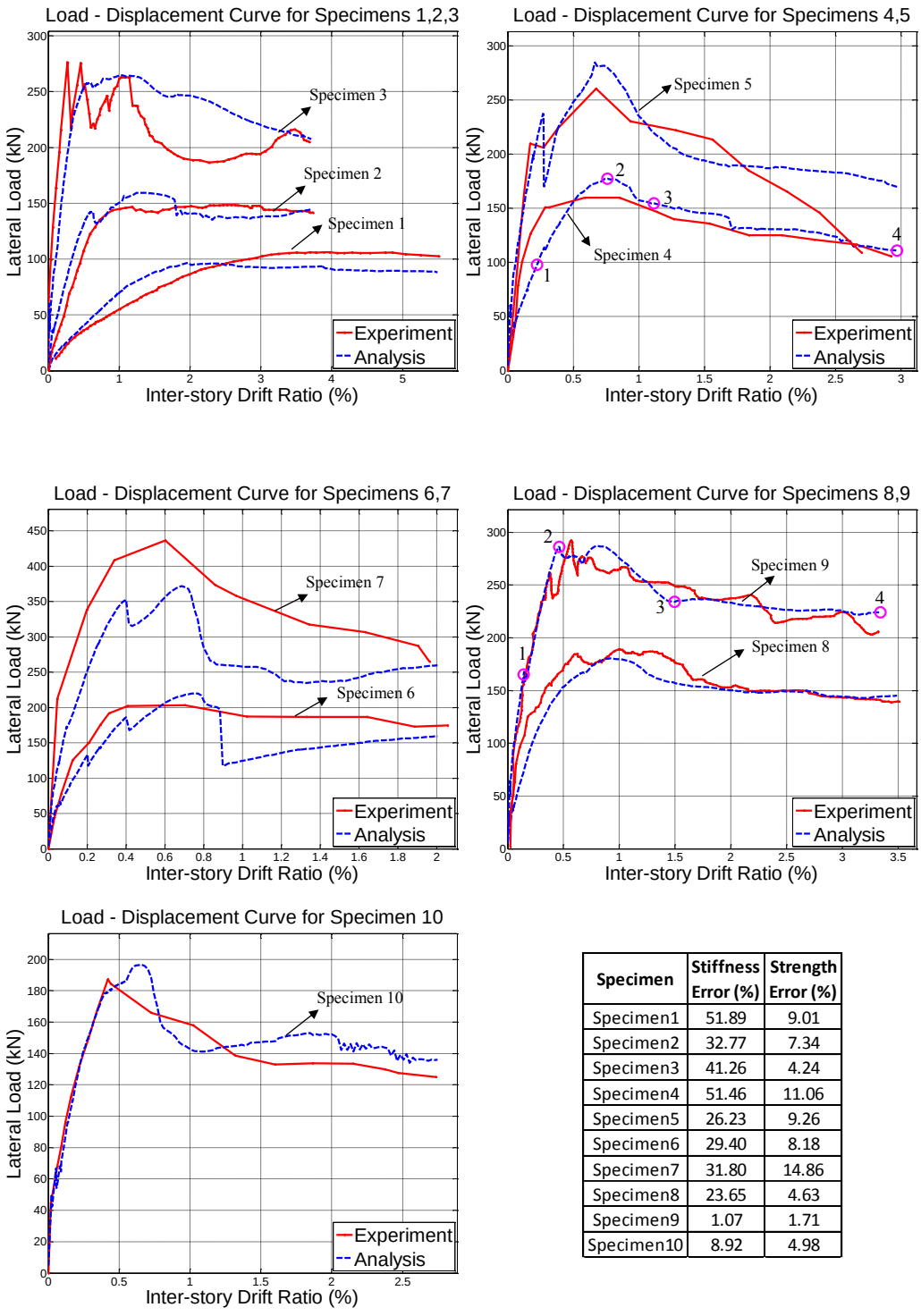

Specimen	Stiffness Error (%)	Strength Error (%)
Specimen1	51.89	9.01
Specimen2	32.77	7.34
Specimen3	41.26	4.24
Specimen4	51.46	11.06
Specimen5	26.23	9.26
Specimen6	29.40	8.18
Specimen7	31.80	14.86
Specimen8	23.65	4.63
Specimen9	1.07	1.71
Specimen10	8.92	4.98

Figure 2.13: Results of Pushover Analyses

The ability of the numerical model to simulate the progressive damage on the reinforced concrete frame and the URM infill wall members and predict the final mode of failure was also investigated. Specimen 4 and 9 were selected for this purpose. The difference of the two frames was that Specimen 4 had a weak infill wall with hollow concrete blocks, where Specimen 9 had a relatively strong infill wall with solid concrete blocks. For the 4 points circled on the pushover curves of each specimen (Figure 2.13), vectors of in-plane principal compressive stresses, crack patterns (disc plots of crack strains) and shear force distribution along boundary columns are given in Table 2.3 and 2.4 respectively. The principal stress vectors help in clearly visualizing the load path within the URM infill wall. The formation and failure of the compression strut mechanism can be observed as the lateral displacement increased. Crack strain plots provide the visual representation of crack patterns in the URM infill wall and the RC frame members. The crack directions indicate the normal direction to the principle tensile strain direction, which was assumed to be the same as the principle tensile stress direction in the material model. Final damage pattern observed for the specimens are also given (Figure 2.14). There is a reasonable agreement between the final damage patterns of the experiment and the simulations for each specimen.

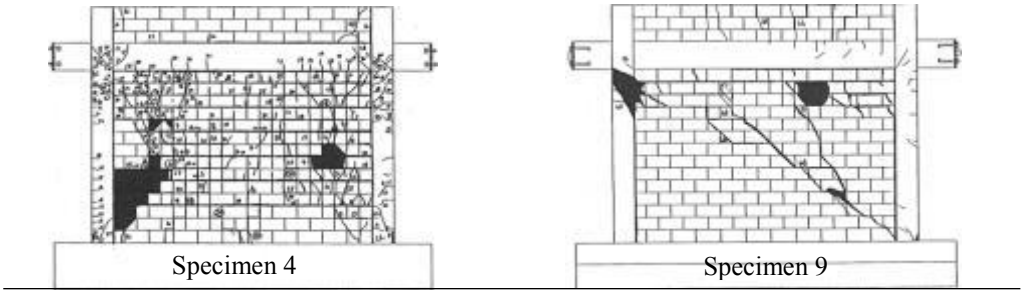

Figure 2.14: Observed Damage in Specimens 4 and 9 (Mehrabi, 1994)

2.6.2. Behavior of Boundary Columns

Simulation results of Specimen 4 revealed that at the first point on the pushover curve (3 mm roof displacement), initial cracks at the URM infill wall occurred. Diagonal compression strut mechanism was formed and shear forces were transferred to the columns (Table 2.3). When 10 mm roof displacement was reached, the first diagonal crack in the URM wall occurred (Table 2.3). This resulted into an off-diagonal strut formation. Shear forces transferred to columns were increased and caused shear induced inclined cracks in RC columns. At point 3 (15 mm roof displacement) which was marked in the pushover curve, increased damage was observed at the URM infill wall and the partial failure

of the compression strut was occurred. The increase in the inter-story drift ratio demand also caused flexural cracking on the columns. At the ultimate roof displacement (40 mm), crushing of the infill wall along with the failure of the strut mechanism was observed. Shear transfer to boundary columns were not significant in this displacement demand. Further flexural cracking was observed in RC members. The failure occurred in the URM infilled RC frame with inclined shear cracks forming on columns as observed in both experimental and simulation results. However, the failure mode was mainly flexural. Flexural crack pattern estimations of the analysis were also in good agreement with the observed damage. Shear force diagrams of the boundary columns were obtained by post processing the stresses at the integration points (Table 2.3). Results show that because of the compressive strut action of the URM infill wall, considerable amount of shear force was transferred to the column ends. However, for the weak URM infill walls and relatively strong bounding frames, the strut capacity was exhausted before the full shear capacity of the columns was reached. This resulted in a relatively ductile response for the considered frame.

Specimen 9 had a relatively strong infill wall relative to its bounding RC frame. Up to the first point (1.9 mm roof displacement) marked on the pushover curve, the frame structure exhibited a stiff behavior, allowing minor displacements and cracking in the URM infill wall. Significant amount of shear force was transferred to column ends. Full concentric diagonal compression strut formation was observed clearly (Table 2.4). At the roof displacement demand of 6.23 mm, first major diagonal crack has occurred. Shear demand induced by the URM infill wall and the column length which was in contact with the infill wall were increased. Inclined shear cracks at RC columns, concentrated at column ends, were observed. The column ends were severely damaged. At the third point on the pushover curve (20.1 mm roof displacement), further crushing of the infill wall and significant strength degradation was observed. It was also observed that crushing of the URM infill at the two opposite corners of the frame caused formation of the short column at the boundary columns. However, shear demand in this case was found be less critical compared to the previous case. Shear force diagrams of boundary columns revealed that forces transferred from URM infill wall were still present and the overall behavior was not purely flexural. At the last point (45 mm roof displacement), inclined cracking were observed at the entire length of the columns and load carrying capacity was further decreased.

Table 2.3: Progression of Damage and Member Force Distributions of During Pushover Analyses: Specimen 4

Lateral Disp. (mm)	In-plane Principal Comp. Stress Vectors	Crack Patterns	Shear Force Diagrams of Columns
3 mm (1)*	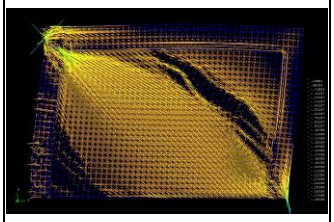	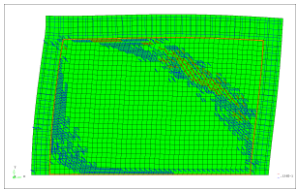	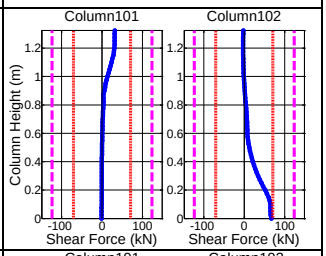
10 mm (2)*	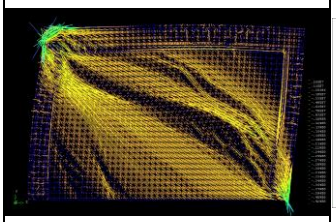	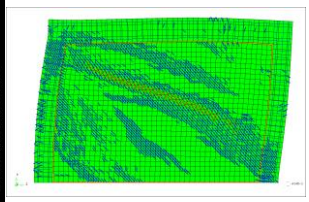	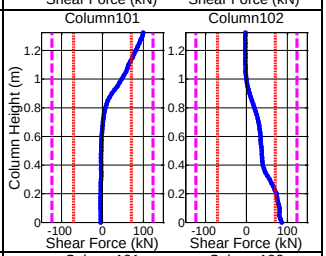
15 mm (3)*	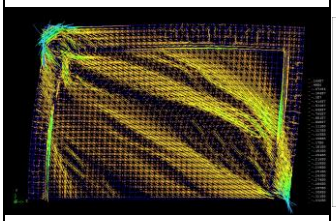	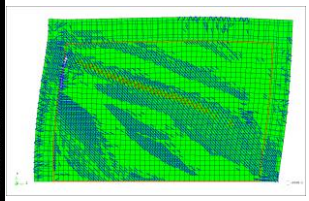	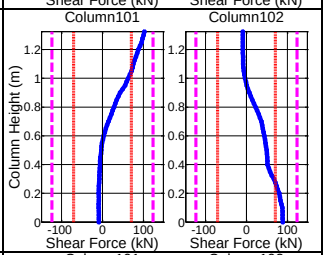
40 mm (4)*	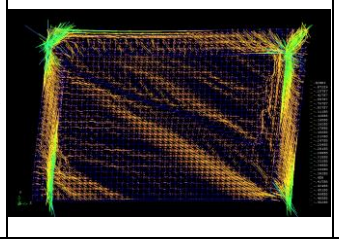	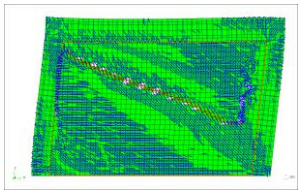	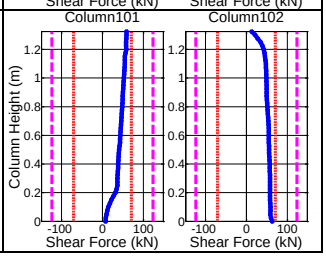

*Points on the load-deformation plots in Figure 2.13
V_{cr}: Concrete shear contribution
V_r: Total Shear Capacity

Table 2.4: Progression of Damage and Member Force Distributions of During Pushover Analyses: Specimen 9

Lateral Disp. (mm)	In-plane Principal Comp. Stress Vectors	Crack Patterns	Shear Force Diagrams of Columns (Demand, Capacity(Vcr), Capacity(Vr))
1.9 mm (1)*	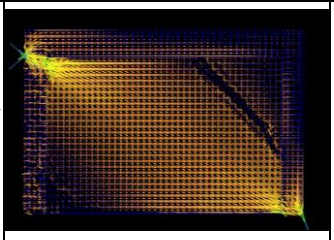	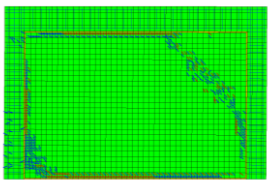	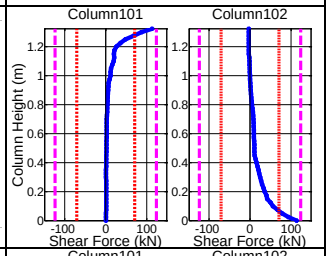
6.23 mm (2)*	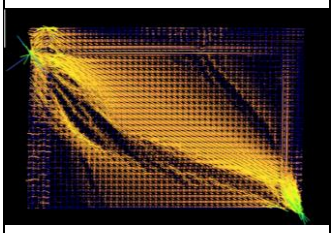	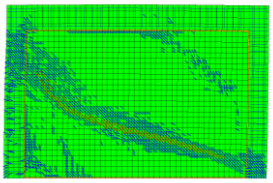	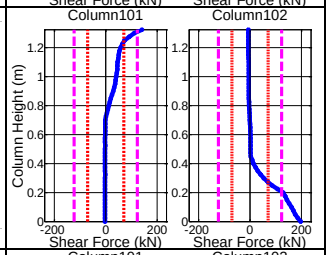
20.1 mm (3)*	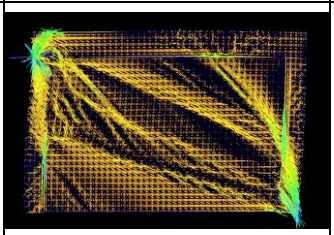	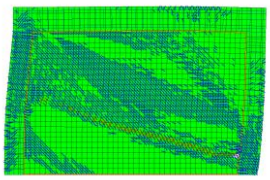	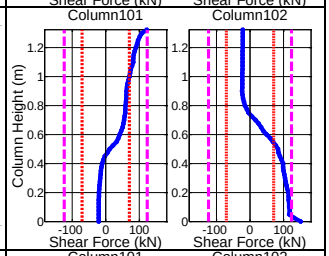
45 mm (4)*	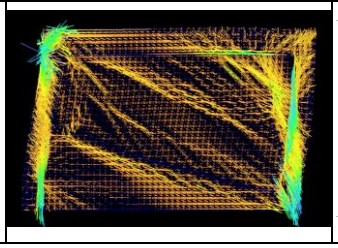	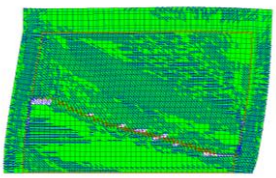	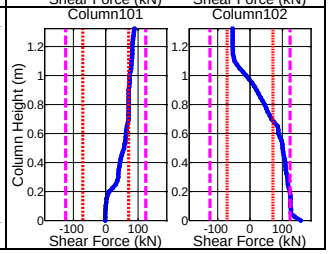

*Points on the load-deformation plots in Figure 2.13
V_{cr}: Concrete shear contribution
V_r: Total Shear Capacity

2.7. Dynamic Analysis of the Code Conforming Test Frame

Results of the simulations presented in the previous section provided significant confidence on the accuracy of the modeling approach. Consecutive nonlinear time history analyses of the test frame for the three ground motions (Figure 2.4) were conducted using previously described FE modeling scheme (Figure 2.9). A damping ratio of 2%

was used in the analysis. The objective of the analysis was to observe the ability of estimating dynamic response of the test frame and to further elaborate on the force distributions on boundary members. The fundamental period of the structure was found as 0.17 sec at the beginning of the analysis. Shear force versus inter-story drift ratio estimations for each story from time history analyses are presented along with the experimental results in Figure 2.15. Inter-story drift ratio time history comparisons of experimental and analytical results for each floor are given in Figure 2.16. It is observed that the numerical simulation results gave accurate estimations for the first story inter-story drifts; however overestimated the inter-story drifts of the second and third story. The lateral strength of the frame was overestimated by 44% in the numerical simulations. For the last ground motion, the finite element model did not capture the period elongation due to the high inelastic action and stiffness degradation (Figure 2.16). This period elongation in the experiment resulted into a decrease in the displacement demand and caused overestimations of the second and third story drifts in the numerical simulations. It can also be observed that the initial stiffness of the system was estimated accurately. However the pinching behavior which was observed in the experiment was not present in the analytical results. This was mainly due to the limitations of the material models, which could not mimic the very complex nonlinear cyclic behavior. First story infill wall diagonal strain estimations of the numerical simulations were also exhibited reasonable results (Figure 2.7), reflecting the ability of the simulations in predicting the wall deformations under reversed dynamic loading.

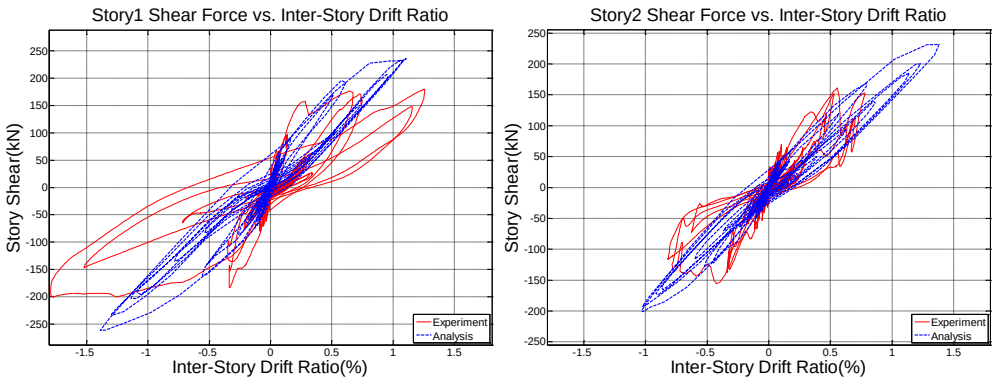

Figure 2.15: Force – Deformation Response Comparison for Specimen 1 (cont'd)

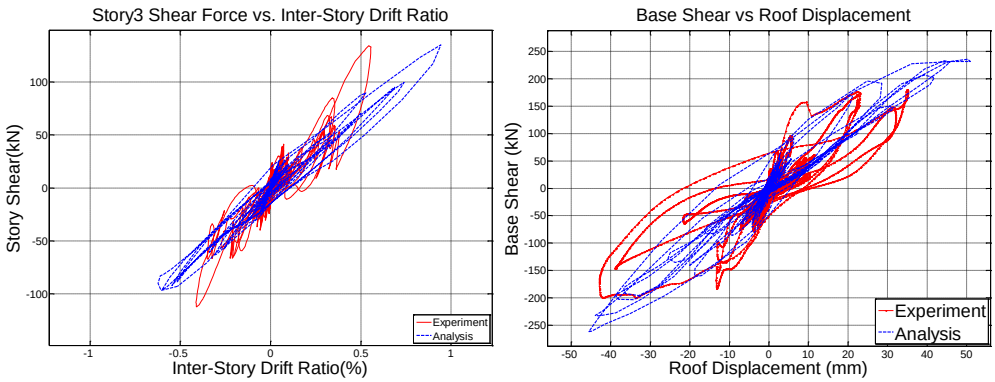

Figure 2.15: Force – Deformation Response Comparison for Specimen 1 (cont'd)

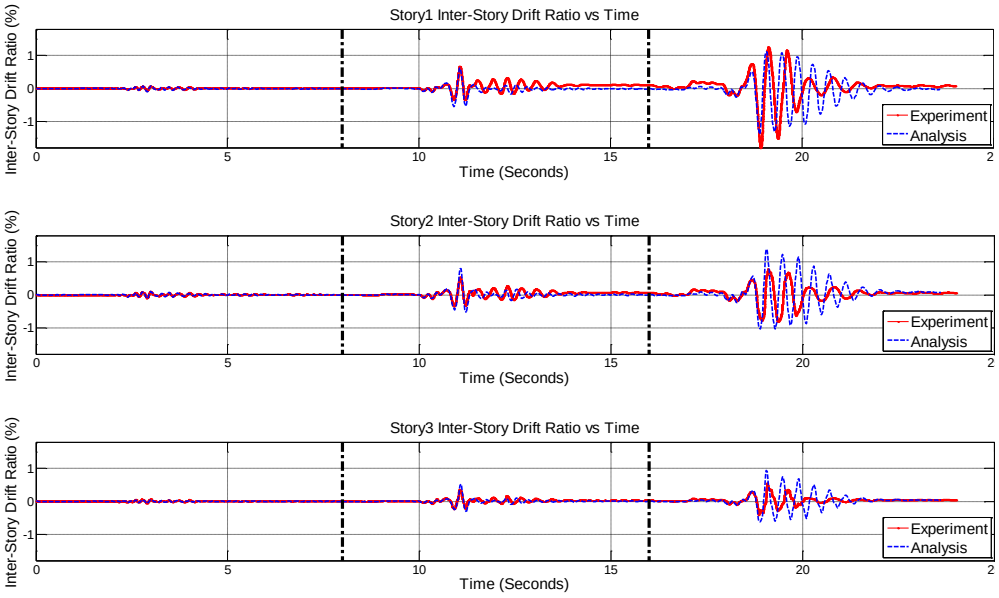

Figure 2.16: Inter-Story Drift Ratio History Comparison for Specimen 1

In addition to the global response parameters such as story shear forces and inter-story drift ratios, local responses such as member-end strains and rotations for the first story columns were also compared. Numerical simulation results revealed that strain and rotation predictions for bottom end of the first story columns was accurate, showing similar trends as the global parameters (Figure 2.17). However, the column top end strains were not estimated as accurate as bottom end strains (Figure 2.18) due to the joint deformations. Moment-curvature responses of the first story exterior columns were also obtained numerically and compared with the experimental results (Figure 2.19). Hysteretic behavior of the experimental and numerical results were found to be similar, however

the unloading regime observed in the experiment was much more pinched than the numerically estimated behavior. This difference which was also encountered in the global force-deformation curves can be attributed to the simplicity of the concrete material model used and the inability of the model to capture bond slip effects. The numerical model was successful in estimating the moment capacities, however failed to capture the ultimate curvature demands accurately obtained from the experimental results. For column 104, the maximum curvature demand occurred in different loading directions for the experiment and the analysis. It should also be stated that the local response parameters of isolated columns were estimated more accurately. Errors of the finite element analysis regarding maximum values of the base shear capacity, roof displacement, inter-story drift ratios, column end rotations, base moments and curvatures are given in Table 2.5.

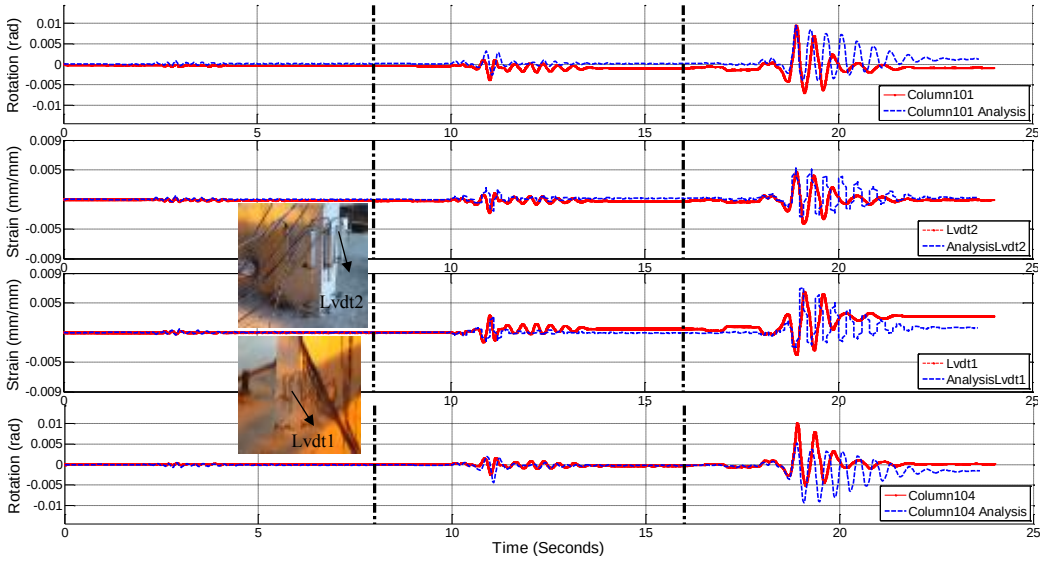

Note: Gauge length is 150 mm for LVDTs at the bottom of the columns and 200 mm for LVDTs at the top of the columns.

Figure 2.17: Local Responses at Bottom of the First Story Columns of Specimen 1

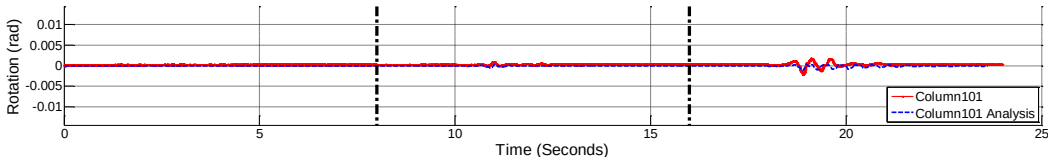

Figure 2.18: Local Responses at Top of the First Story Columns of Specimen 1(cont'd)

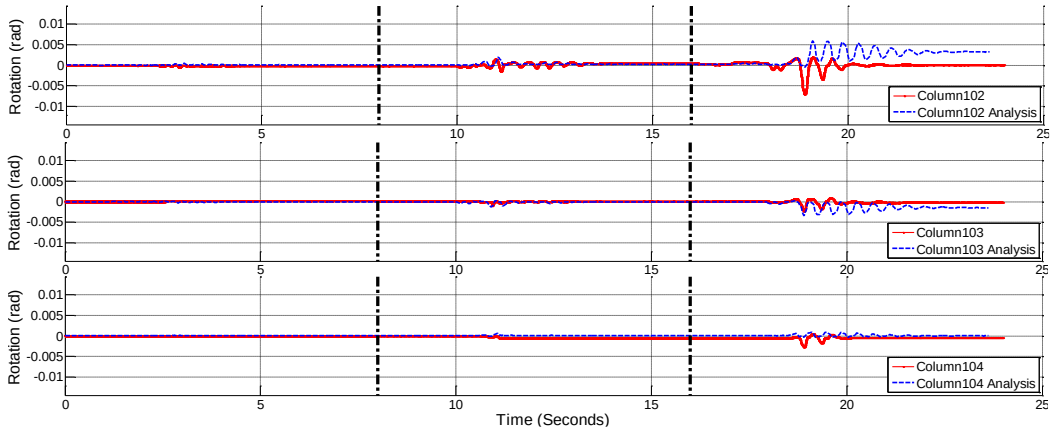

Note: Gauge length is 150 mm for LVDTs at the bottom of the columns and 200 mm for LVDTs at the top of the columns.

Figure 2.18: Local Responses at Top of the First Story Columns of Specimen 1(cont'd)

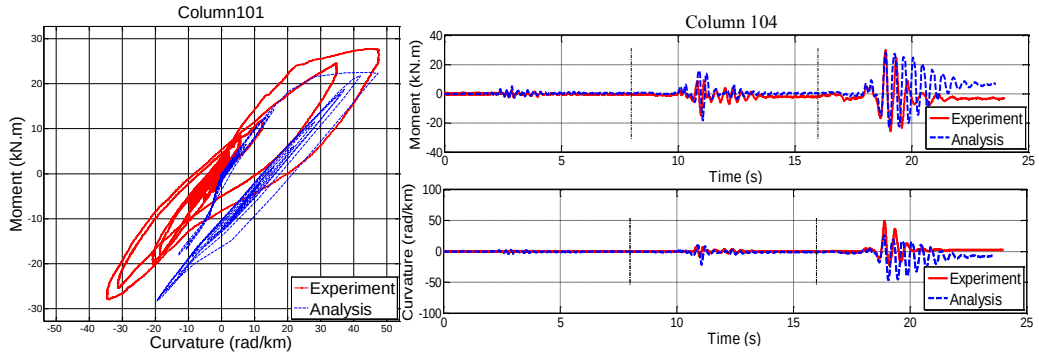

Figure 2.19: Moment – Curvature Relationships for Exterior Columns

Table 2.5: Errors (%) of FE Analysis at Maximum Points for Specimen 1 (cont'd)

			(+) dir.	(-) dir.
Base Shear Capacity			44.2	44.3
Roof Displacement			45	6.04
Inter-Story Drift Ratio		Story 1	11.9	22.5
		Story 2	77	26.1
		Story 3	69.7	50.8
Column End Rotations	**Column 101**	bottom	0.1	43.7
		top	94.7	77.6
	Column 102 (strain)*	bottom	0.1	2.0
		top	50	97.0

Table 2.5: Errors (%) of FE Analysis at Maximum Points for Specimen 1 (cont'd)

Column End Rotations	**Column 103** (strain)*	bottom	0.3	0.8
		top	96.6	56.9
	Column 104	bottom	48.5	83.4
		top	77.2	95.4
Moment		Column 101	18.8	1.3
		Column 104	5.6	12.8
Curvature		Column 101	0.1	43.9
		Column 104	47.2	119.5
Diagonal Wall Strain		Wall1	37.6	32.6

*Rotation data was not available.
(+) dir.: positive loading direction, (-) dir.: negative loading direction

2.8. Forces on Columns Adjacent to Infill Walls

Using the numerical simulation results, shear force diagrams of the first story columns were obtained at the peak deformation instant (Figure 2.20). Shear force was found to be constant along the exterior columns and linearly varying along the columns adjacent to infill wall panels. This reveals that the compression strut induced a nearly uniform distributed load on the boundary columns. The magnitude of the distributed load and the corresponding strut width, and the shear demand on column ends were calculated from the shear force diagrams as shown in Figure 2.21. Here, the length which the shear force varied linearly was considered to be under uniform distributed loading transferred from the infill wall. Strut width is obtained by taking the average of the two column lengths where the distributed load was acting. Magnitude of the uniform distributed load was obtained by calculating the slope of the shear diagram. Maximum shear demands at the first story columns were calculated as 45 kN and 67 kN for the exterior columns 101 and 104 respectively and 117 kN for the boundary columns. Shear demand at one boundary column (102) was found to be larger than the shear capacity of the column which was computed as 78.2 kN for the confined region using:

$$V_c = 0.52 f_{ctd} b_w d (1 + \frac{\gamma N_d}{A_c}), \tag{2.4}$$

$$V_w = \frac{A_{sw}}{s} f_{ywd} d \tag{2.5}$$

where V_c is the concrete contribution, b_w and d are the dimensions of the column section, N_d is the design axial load and γ isa modification factor for the axial load. A_c and A_{sw} represents the areas of the concrete section and transverse steel respectively. Tensile strength of concrete and yield strength of transverse steel is denoted as f_{ctd} and f_{ywd} and s is used to denote the spacing of stirrups. The columns were designed according to the capacity design principle of TEC 2007 excluding the presence of infill walls. Con-

sidering the computed shear demands at the boundary columns, it can be stated that the boundary column 102 is prone to shear failure and it can no longer be classified as a ductile member.

The accuracy of the ASCE/SEI 41-06 in estimating the strut width and the required shear strength of column members adjacent to infill walls was also investigated. The strut width was computed according to:

$$a = 0.175(\lambda_1 h_{col})^{-0.4} r_{rinf} \tag{2.6}$$

where

$$\lambda_1 = \left[E_{me} \frac{t_{inf} sin2\theta}{4 E_{fe} I_{col} h_{inf}} \right]^{\frac{1}{4}} \tag{2.7}$$

In equations 2.6 and 2.7, a stands for the strut with, h_{col} for the column height, r_{rinf} for the diagonal length of the infill panel, t_{inf} for the thickness of the infill wall and h_{inf} for the height of the infill. E_{me} and E_{fe} represent the elastic modulus of masonry infill wall and frame materials respectively and I_{col} represents the moment of inertia of the column section in its bending direction. θ is the angle whose tangent is the infill wall height to length aspect ratio. It is observed that the strut width estimated by ASCE/SEI 41-06 (0.243 m) is considerably small compared to the analysis results (~1.025 m) resulting in underestimation of the strut stiffness in macro models.

The shear forces computed based on a short column formation along the vertical component of the strut width using:

$$V_d = \frac{M_1 + M_2}{l_{ceff}} \tag{2.8}$$

where

$$l_{ceff} = \frac{a}{cos\theta} \tag{2.9}$$

Here, l_{ceff} is the reduced column length due to the contact from the infill wall and M_1 and M_2 are expected the moment capacities at the top and bottom of the column with the reduced length. The shear force resulted from the short column formation was computed as 171 kN. This force is larger than the estimated shear force from the simulation, hence can be accepted as conservative for the purposes of boundary column evaluation. On the other hand, the horizontal component of the strut force was estimated from:

$$V_{inf} = 0.4 A_{inf} \tag{2.10}$$

where A_{inf} is the area of net mortared/grouted section in the infill wall. For the shear strength, lower-bound values recommended by ASCE/SEI 41-06 were used due to the lack of masonry shear tests on mortar specimens. The shear force which will be transferred from the infill was estimated as 74.4 kN. This shear force is found to be smaller compared with the actual shear demand obtained from the simulations (117 kN) resulting in an unsafe estimation.

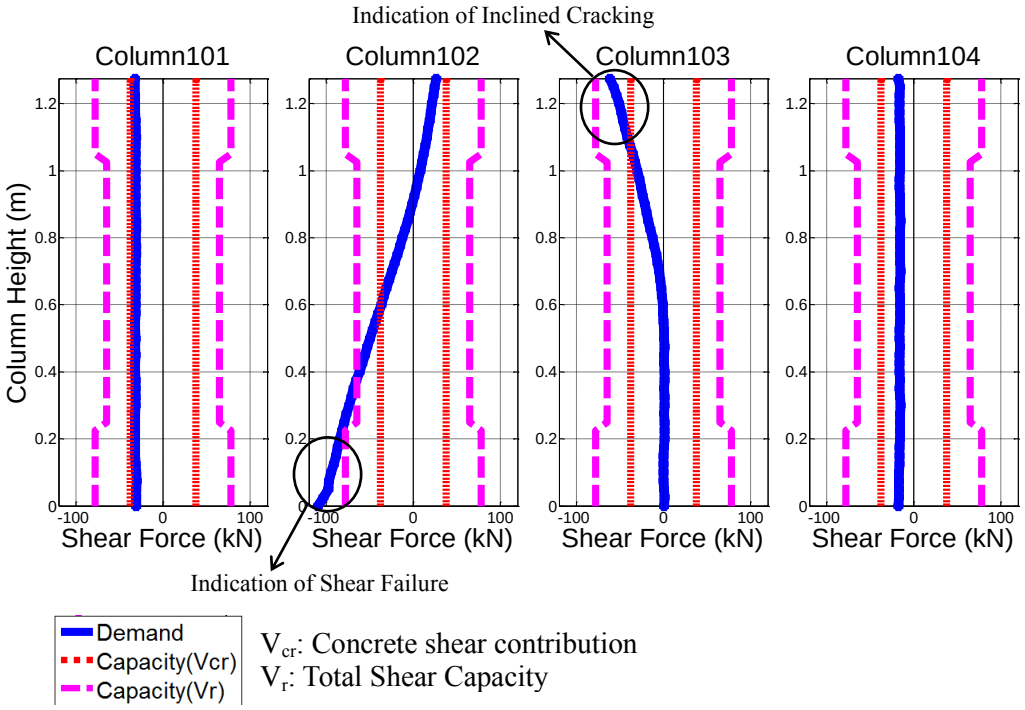

Figure 2.20: Shear Force Diagrams of the First Story Columns of Specimen 1 at Peak Deformation

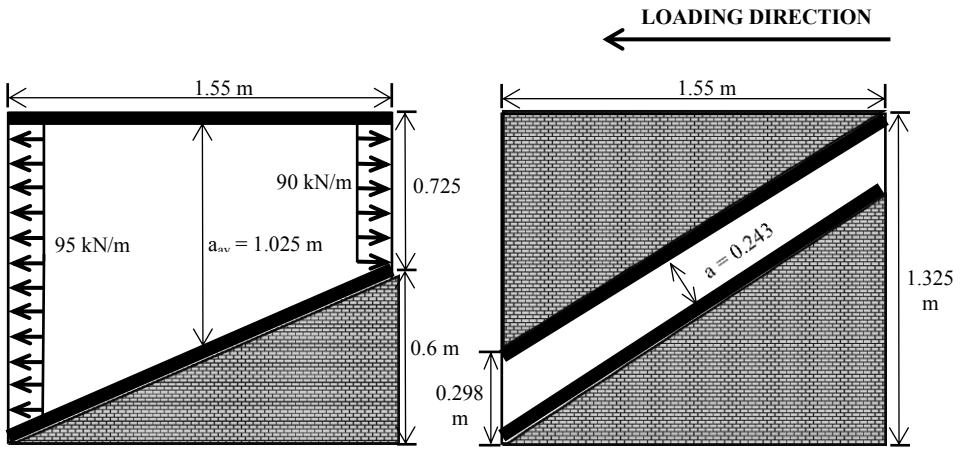

a) Simulation Results *b) ASCE/SEI 41-06 Estimation*

Figure 2.21: Properties of the Compression Strut (Specimen 1)

From the simulations conducted on frames with weak infill panels, it is observed that considerable amount of shear force is transferred to the boundary columns. It is clear that these members cannot be clasified and evaluated as pure flexural members since the shear force on those members greatly influence the behavior and failure mode. For the infilled frames with weak infill panels considered here, shear failure of the columns did not occur due to the forces transferred from the strut mechanism. However, critical amount of shear force transferred resulted in significant shear damage on the columns, contradicting with the design philosophy of the members. For the frames in question, short column formation following crushing of the infill wall was found to be not critical. Estimations of ASCE/SEI 41-06 is found unsatisfactory regarding the probable shear forces transferred to columns.

Considering the simulations on frames with weak infill panels, masonry infilled frames exhibited nearly a linear elastic behavior up to first cracking in the infill wall. This crack was in the form of a diagonal crack, corresponding to an inter-story drift of about 0.1 - 0.3 %. After the first cracking, further cracking of the infill wall and flexural crack formation at the RC members was observed. Maximum shear force in columns developed right before the capacity was reached (~0.75% inter-story drift).

CHAPTER 3

DEFICIENT FRAME AND THE ASSESSMENT OF EXAMINED FRAMES

The seismic performance of a deficient i.e. code incompliant RC frame with URM infill walls is examined in this chapter. The chapter consists of two main parts. In the first part, the properties of the test frame, experimental and analytical results are discussed. Seismic assessment of the code compliant frame along with the deficient frame are addressed and discussed in the second part.

First, all the properties of the test frame are presented. Then the results of the PsD experiment under three levels of ground motion are discussed. The presented results include inter-story drift ratios and force deformation responses of each story. Identified natural vibration period and damping ratio histories are also presented. Dynamic analysis results under three levels of ground motion are presented and the accuracy of the model to simulate both global and local demand parameters is investigated. Results of the dynamic analysis are given together with the experimental results. These results include force deformation relationships and inter-story drift ratios at each story, strain and rotation demands at the plastic hinge regions of column members and moment-curvature relationships of exterior columns. Forces on boundary columns in the simulations are examined along with the strut properties and shear demand on boundary columns. Comparisons of the results are made with the code complaint frame.

The only code or guideline that provides performance limits for URM infill walls and their boundary frame members in the seismic response analysis and assessment is ASCE/SEI 41-06. Therefore, seismic assessment procedure in ASCE/SEI 41-06 is summarized and the recommendations about infill walls and infilled frames are interpreted. Assessment results for the two specimens (Specimen 1 and Specimen 2 in this study) and 9 infilled specimens tested by Mehrabi (1994) are presented. The obtained results are compared with the observed behavior and the accuracy and safety of the procedure proposed by ASCE/SEI 41-06 is discussed.

3.1. Properties of Specimen 2

The ½ scaled three story-three bay reinforced concrete frame with masonry infill walls at its central bay test was selected from a typical interior frame of an RC prototype building (Figure 2.1.a). Geometric properties of the prototype building and the test frame were identical as the ones described in Chapter 1. The building was designed to reflect the most critical and common deficiencies present in Turkey's current building stock. These deficiencies include using plain bars instead of deformed bars, low material strengths, having stronger beams relative to columns and insufficient transverse reinforcement at the member end regions and joints. Gravity load applied by the help of steel blocks was the same as Specimen 1. Column and beam dimensions were same as Specimen 1. Reinforcement details of the column and beams are shown in Figure 3.1. No transverse reinforcement was used in the beam-column joints. Detailing of the reinforcement was the same in both middle and end regions of the columns. Plain bars were used for both longitudinal and transverse reinforcement. For the transverse reinforcement, 4 mm plain bars were used with no intermediate ties. End region of beams were confined properly to have strong beam-weak column condition to realistically represent a deficient frame (Figure 3.1). Infill wall thickness, material and construction technique were the same as Specimen 1. Uniaxial compressive tests on concrete cylinder specimens revealed an average compressive strength of 13.6 MPa. The average uniaxial compressive strength of mortar and plaster were 8.5 MPa and the hollow clay brick units had a uniaxial compressive strength of 8.5 MPa. 4 mm plain bars which were used as transverse reinforcement had a yield strength of 240 MPa and ultimate strength of 340 MPa. 8 mm plain bars were used as longitudinal reinforcement with a yield strength of 320 MPa and an ultimate strength of 460 MPa. 10 mm plain bars, which were used as longitudinal reinforcement, had a yield strength of 355 MPa and an ultimate strength of 555 MPa. Previously explained test setup, testing methodology, ground motions and instrumentation were used in this test.

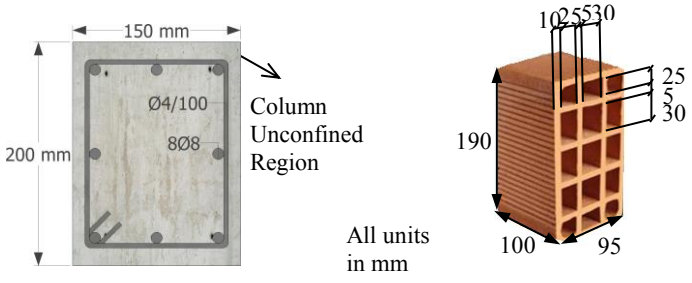

Figure 3.1: Section Properties of the Specimen 1 (cont'd)

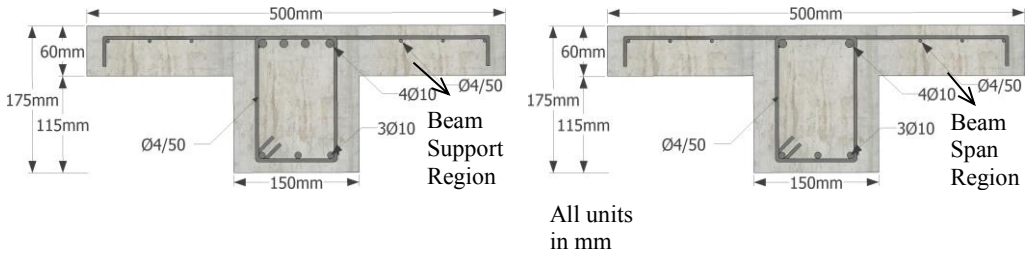

Figure 3.1: Section Properties of the Specimen 1 (cont'd)

3.2. Experimental Results

The inter-story drift ratios of the three stories along with the damage patterns, which were observed during the peak deformation instants of the experiment, are given in Figure 3.2. Force-deformation relationships of each story in the form of story shear versus inter-story drift ratio are given in Figure 3.3. Force-displacement curves of each story reveal that the load carrying capacity of the frame dropped after the shear failure of the first story boundary column at the end of the tests. The load carrying capacity of the frame decreased about 20% in both loading directions. Strength drop in the second and third stories did not occur due to the strong infill wall and small story drifts.

D1 ground motion caused flexural cracking of the beams and some minor joint damage. Significant cracking of the first story frame-infill wall interface was observed in D2 ground motion. Inclined shear cracks formed at the top of the boundary columns without any serious damage in the infill wall. Widening of the flexural cracks in RC members was also observed (Figure 3.2). Maximum inter-story drift ratio of the first story at the end of D2 ground motion was about 0.5% at a roof displacement of 20 mm. D4 ground motion caused severe damage in RC members. Boundary columns suffered severe inclined cracking from the shear forces transferred from the infill walls. Shear capacity provided was sufficient when flexural yielding of the column ends was considered. This can be further supported by the experimental results of the bare frames with the same properties. Detailed experimental and analytical research on such test frames can be found in Mutlu (2012). Existing inclined cracks at the column ends turned into very wide, see through cracks and buckling of the longitudinal reinforcement was also observed. Isolated column members did not suffer any heavy damage, however wide flexural cracks were monitored in those members. Spalling of the cover concrete was also observed. The strong infill walls did not exhibit any diagonal cracking or horizontal sliding. Minor corner crushing occurred in the first story infill wall. Separation of the first story infill wall from the RC frame was observed, however the out-of-plane stability of the wall was not jeopardized. Maximum inter-story drift ratio of the first story at the end of D4 earthquake was about 1.85% corresponding to a roof displacement of 56 mm. Maximum base shear demand measured during experiment was 188 kN. Base shear

versus roof displacement responses for the D1, D2 and D4 ground motions are presented in Figure 3.3. Diagonal wall strains measured in the first and second story infill wall diagonals are given in Figure 3.4. Results concerning the local demand parameters such as member-end rotations and curvatures are presented and discussed in the numerical simulations part.

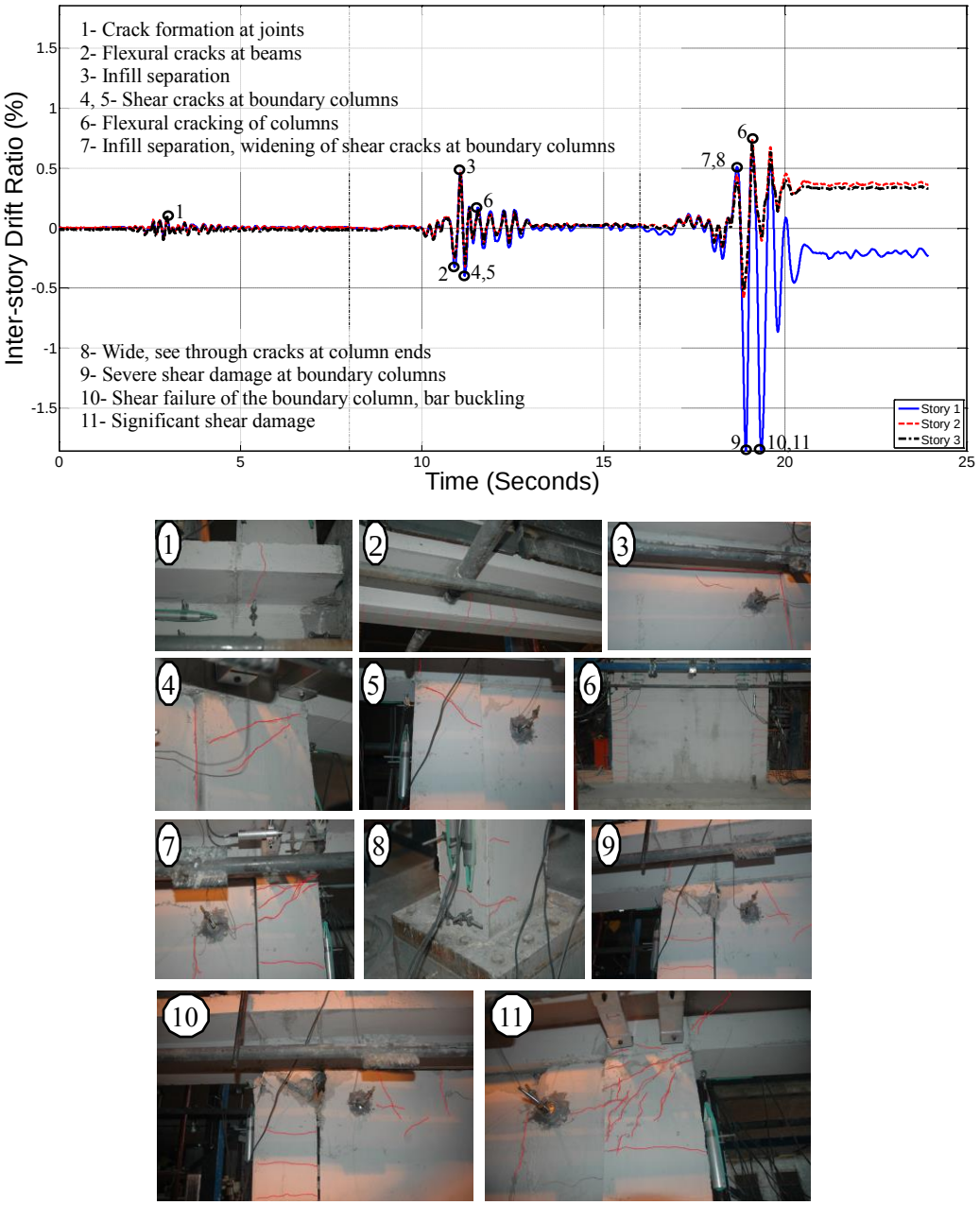

Figure 3.2: Inter-Story Drift Ratio Response along with Damage Patterns for Specimen 2

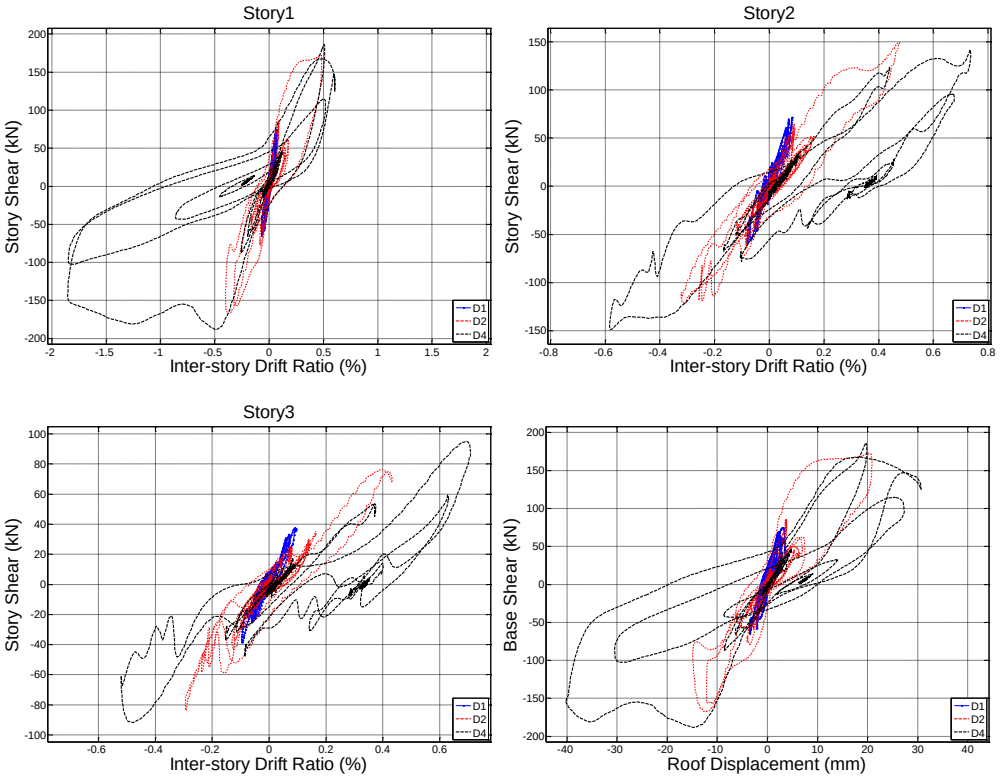

Figure 3.3: Force- Deformation Response for Specimen 2

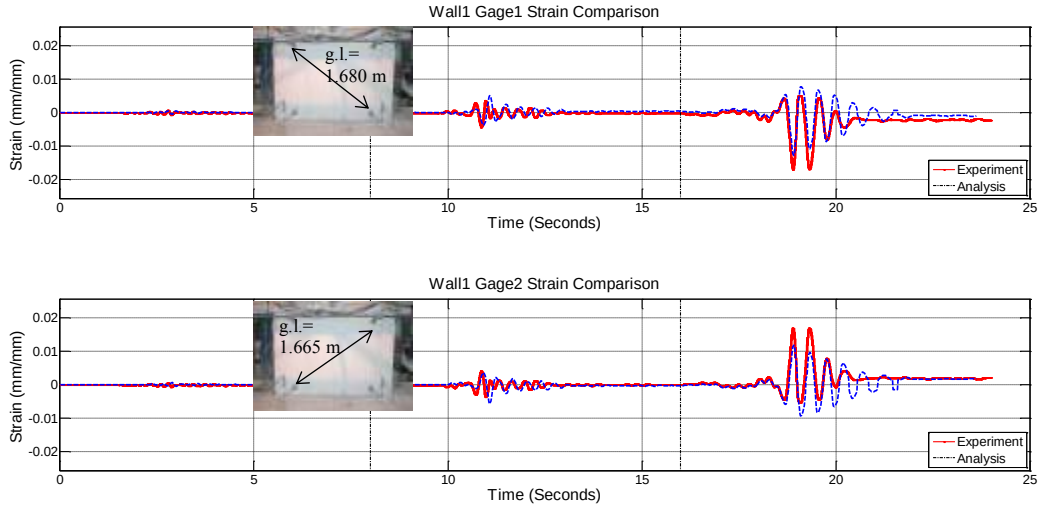

Figure 3.4: Diagonal Wall Strain Response for Specimen 2 (cont'd)

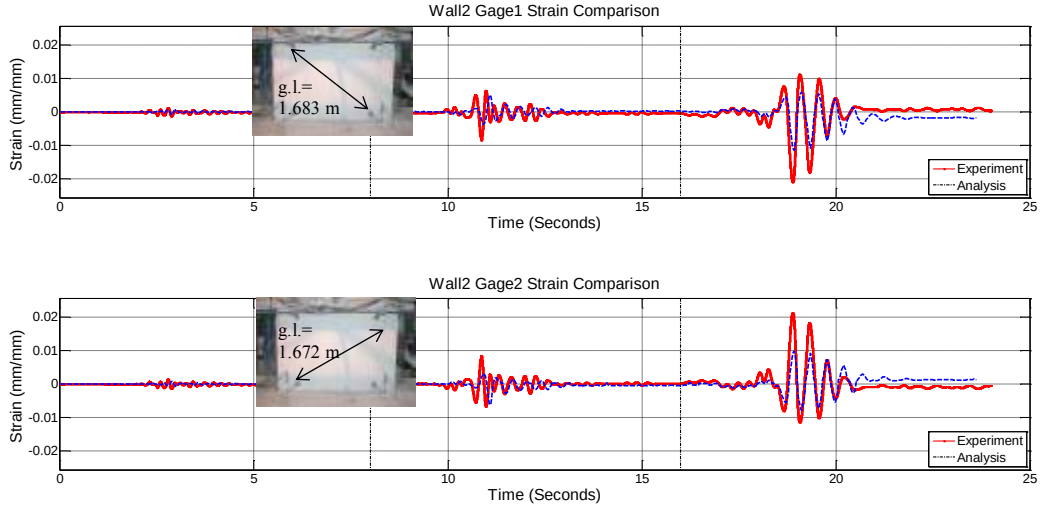

g.l.: gauge length

Figure 3.4: Diagonal Wall Strain Response for Specimen 2 (cont'd)

3.3. Identification of Dynamic Parameters

Identification of dynamic parameters of the test frame, namely the time dependent vibration periods and damping ratios is obtained using the previously explained procedure by Molina et al. (1999). Results of the identification are given in Figure 3.5. Identification results reveal that the first mode period of the frame was about 0.2 sec at the beginning of the test and stayed constant until the end of D1 earthquake. The results were numerically stable, meaning no significant nonlinearity occurred during D1 earthquake. At the end of D2 earthquake, fundamental period elongated to about 0.3 seconds. During D4 earthquake, significant damage on the structure caused the period to elongate even more. At the end of D4 earthquake, period was about 0.5 sec. Minor damage in the infill wall and limited ductility of the frame prevented the period from further elongations. Identified damping ratio of the structure was about 5% at the beginning of the experiment. It is observed that the damping was about 15% during the rest of the experiment, with several peaks at the instants of highly nonlinear actions.

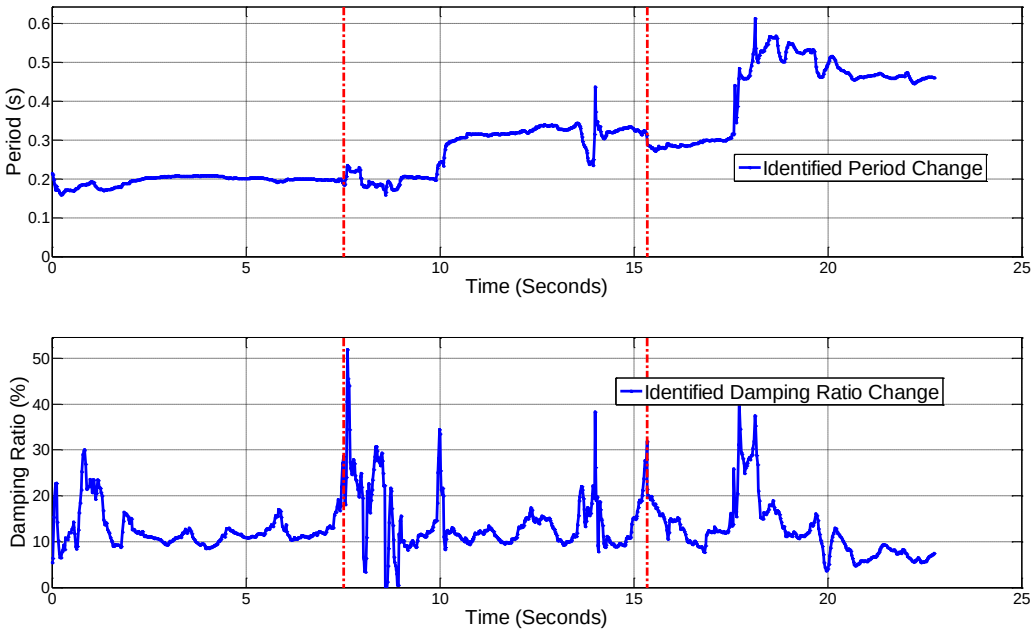

Figure 3.5: Identified Period and Damping Ratio for Specimen 2

3.4. Dynamic Analysis of the Deficient Test Frame

For the dynamic analysis of the test frame, the modeling approach explained previously in Section 2.6 was employed (Figure 2.9). The test frame was modeled as a continuum in plane stress in DIANA (2008). All the material properties used in the simulations are given in Table 3.1. Consecutive nonlinear time history analyses of the deficient test frame for the three ground motions (Figure 2.2) were conducted and a damping ratio of 2% was assumed. The linear eigenvalue analysis revealed a fundamental period of 0.17 sec. Analysis results for story shear force versus inter-story drift ratio for each story and base shear versus roof displacement are presented along with the experimental results (Figure 3.6). The accuracy of the finite element model in estimating the global response parameters, namely base shear capacity, roof displacement and inter-story drift ratios is investigated. The simulation results exhibited accurate estimations in terms of global response parameters. Hysteretic behavior obtained in the simulations resembled the behavior observed in the experiment. Shear capacities of each story and the base shear capacity were estimated accurately. There is also reasonable agreement between the initial stiffness obtained from the simulations and the experiment. The period elongation in the experiment was not observed in the analysis, which resulted in an overestimation in the displacement demand and caused inaccurate estimation of the roof displacement in one loading direction. Similar to the first specimen, the inter-story drift ratio of the

first story was estimated accurately; however the simulation results overestimated the inter-story drifts of the second and third stories. The third story inter-story drift ratio, on the other hand, was overestimated in one direction and underestimated in the other direction. Inter-story drift ratio time histories are also presented along with the experimental results in Figure 3.7.

Table 3.1: Material Properties Used in Numerical Simulations of Specimen 2

Wall Medium		**Mortar (Interfaces)**		
Elastic Modulus E_c (MPa)	850	Normal Stiffness K_{nn} (N/m^3)	1.25×10^{12}	
Compressive Strength f'_c (MPa)	8.5	Tangential Stiffness K_{tt} (N/m^3)	1.25×10^{12}	
Tensile Strength f_{ct} (MPa)	0.4	Cohesion c (MPa)	0.5	
Fracture Energy (N.m)	24890	Friction Angle (tanφ)	0.5	
Concrete		**Reinforcing Steel**		
		Reinforcing Bar	**Yield Strength (MPa)**	**Ultimate Strength (MPa)**
Elastic Modulus E_c (MPa)	17517	4 mm plain bars	240	340
Compressive Strength f'_c (MPa)	13.6	8 mm plain bars	320	460
Tensile Strength f_{ct} (MPa)	1.3	10 mm plain bars	355	555

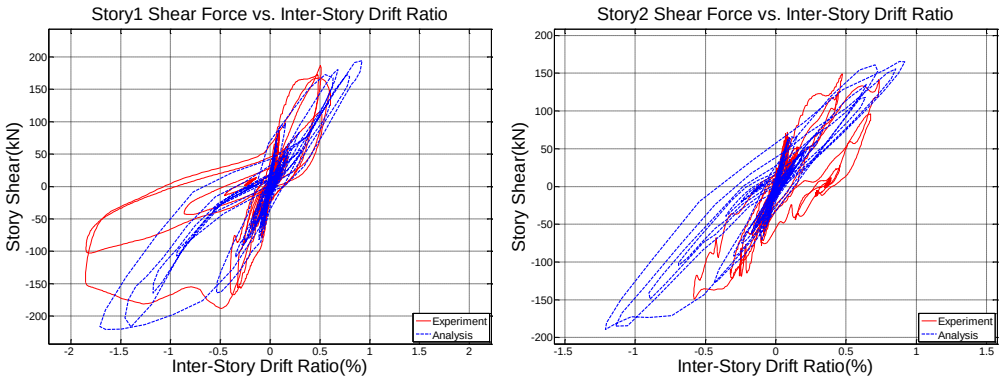

Figure 3.6: Force – Deformation Response Comparison for Specimen 2 (cont'd)

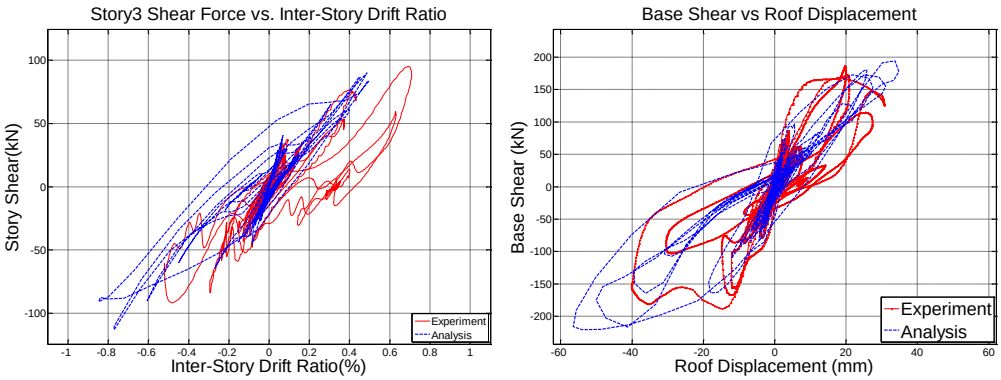

Figure 3.6. Force – Deformation Response Comparison for Specimen 2 (cont'd)

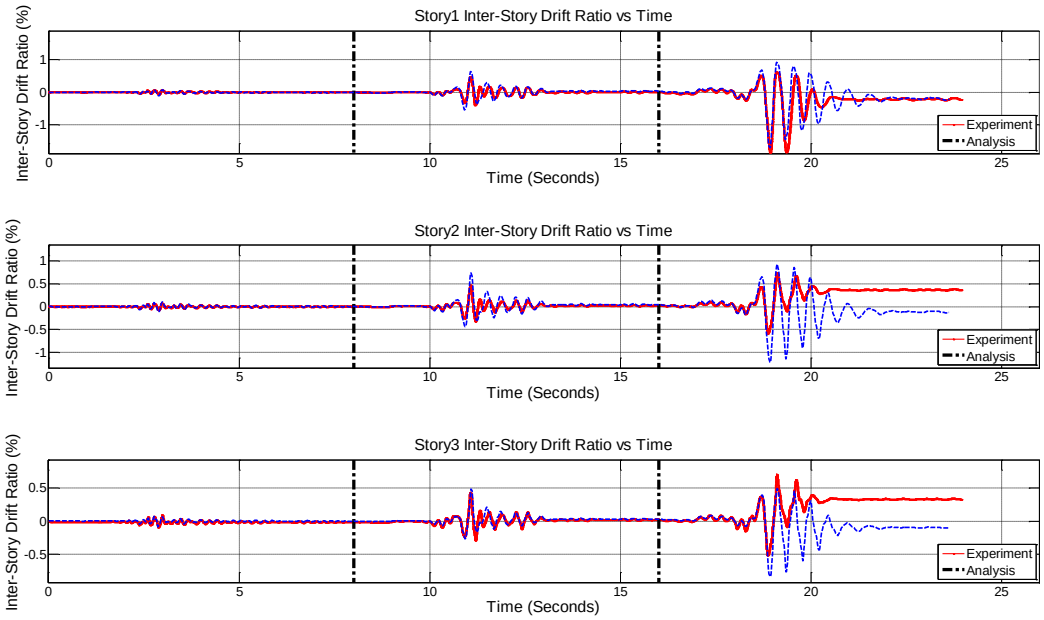

Figure 3.7. Inter-Story Drift Ratio History Comparison for Specimen 2

Comparisons of the local responses, namely the member-end rotations, strains and curvatures of the first story columns were also conducted. Results regarding the first story member-end rotations are given in Figure 3.8 and Figure 3.9. The numerical simulation results were not as successful as the results for the code conforming frame, implying that the estimation of the local demand parameters becomes a more challenging task for deficient frames. Bottom end responses were estimated with smaller errors compared to top end responses which was affected by joint deformations. It should also be noted that the maximum values of member-end rotations and strains were estimated accurately,

which stands important in the assessment of the members. Similar to Specimen 1, local deformation demand estimations for column 104 exhibited large errors. Diagonal wall strains of the first and second story infill walls were also extracted from the analysis and compared with the experimental data (Figure 3.4). Simulation of the cyclic behavior of the infill wall diagonals is found successful for the first story where the diagonal strain in the second story infill wall was underestimated. Errors of the finite element analysis regarding maximum values of the base shear capacity, roof displacement, inter-story drift ratios, column end rotations and curvatures are given in Table 3.2.

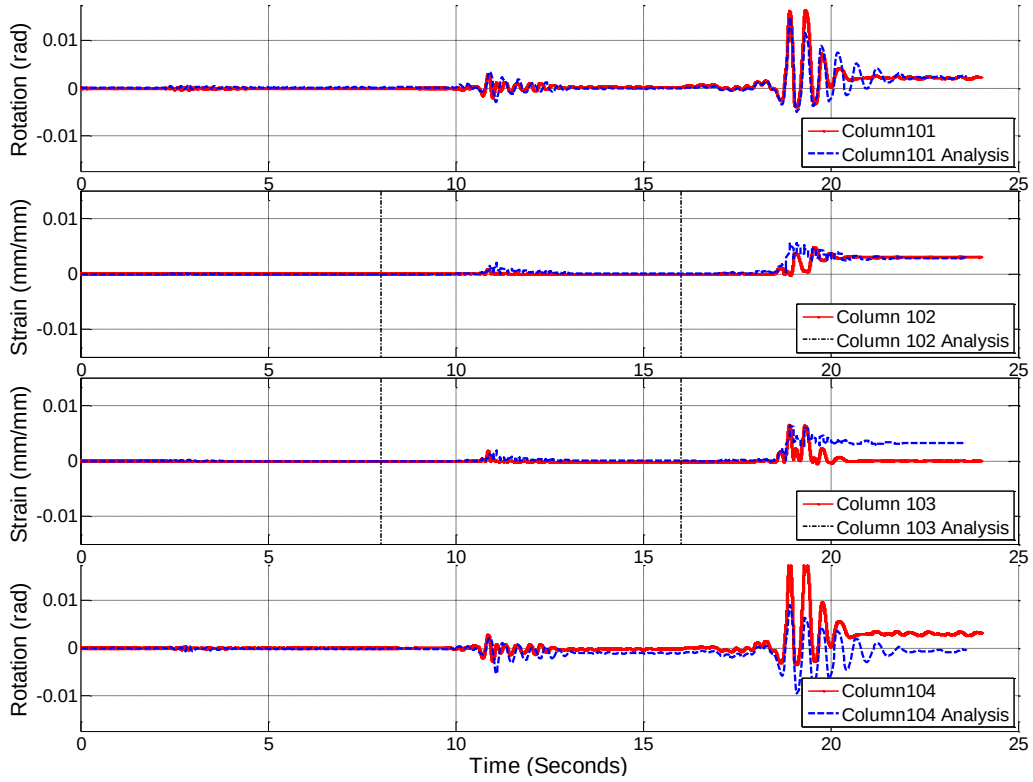

Figure 3.8: Local Responses at Bottom of the First Story Columns of Specimen 2

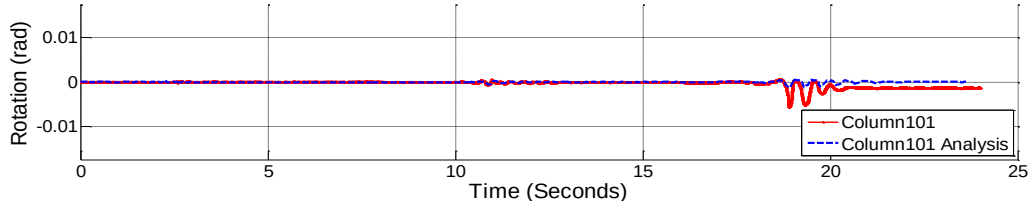

Figure 3.9: Local Responses at Top of the First Story Columns of Specimen 2 (cont'd)

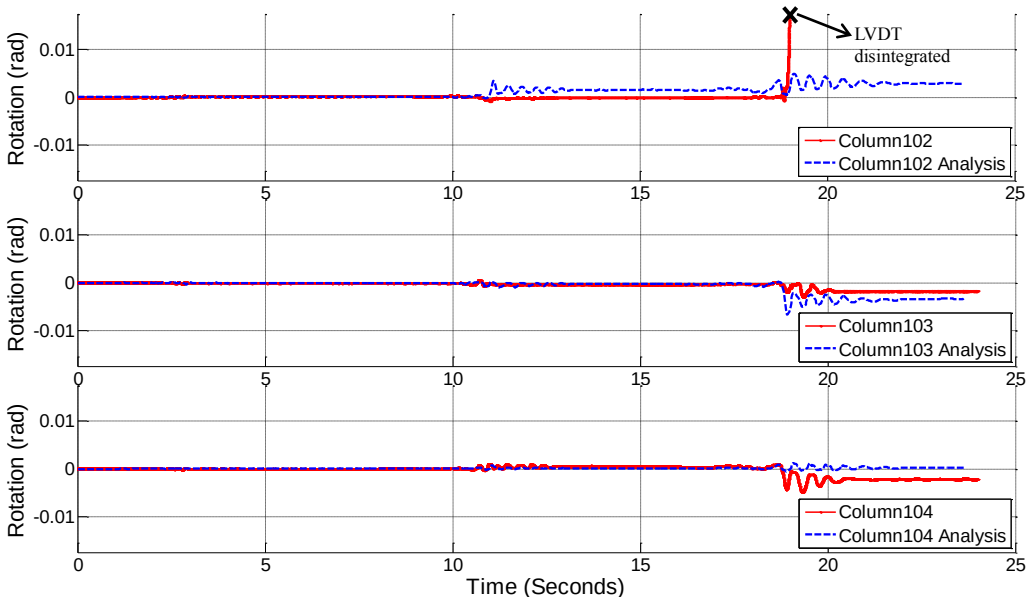

Figure 3.9: Local Responses at Top of the First Story Columns of Specimen 2 (cont'd)

Table 3.2. Errors of FE Analysis at Maximum Points for Specimen 2

			Error (%)	
			(+) dir.	(-) dir.
Base Shear Capacity			4.2	17.2
Roof Displacement			13.1	40.3
Inter-Story Drift Ratio		Story 1	52.2	7.7
		Story 2	24.7	107.7
		Story 3	30.0	62.8
Column End Rotations	**Column 101**	bottom	9.8	26.9
		top	10.8	77.2
	Column 102 (strain)*	bottom	0.5	1.0
		top	95.4	79.4
	Column 103 (strain)*	bottom	0.4	1.0
		top	70.7	129.4
	Column 104	bottom	52.6	175.1
		top	67.0	89.1
Moment		Column 101	**	**
		Column 104	**	**
Curvature		Column 101	6.09	7.5
		Column 104	53.4	203.5
Diagonal Wall Strain		Wall 1 - Gage 1	49.6	24.8
		Wall 1 - Gage 2	127.9	45.2
		Wall 2 - Gage 1	65.4	122.2
		Wall 2 - Gage 2	42.3	50.2

*Rotation data was not available. **Acquired data is not correct.
(+) dir.: positive loading direction, (-) dir.: negative loading direction

3.5. Forces on Columns Adjacent to Infill Walls

Shear force diagrams of the first story columns were obtained at the peak deformation instant (Figure 3.10). Shear diagrams were similar to the ones obtained for Specimen 1. Shear forces along the length of the exterior columns were found to be constant, whereas it was found to be almost linearly varying along the height of the columns adjacent to infill walls. This linearly varying shear force diagrams can be interpreted as a result of the presence of uniformly distributed forces which were acting on boundary columns. The magnitude of the distributed load and the corresponding strut width, and the shear demand on column ends were calculated from the shear diagrams. Because of the frame-infill wall interaction, significant shear force was transferred to the boundary columns. Maximum shear demands occurred at the first story columns were 24 kN for column 101, 93 kN for column 102, 51 kN for column 103 and 14 kN for column 104 at the peak deformation. Calculated shear demands at the boundary columns from simulation results were found to be larger than the shear capacity calculated according to Equations 2.4 and 2.5. Considering high shear demands on boundary columns and insufficient shear design of the test frame, it should be noted that the assessment of these columns require great care. Buildings with insufficient confinement and shear reinforcement become more vulnerable to earthquakes since brittle shear failure of the boundary columns is critical.

For the seismically deficient frame, the accuracy of ASCE/SEI 41-06 in estimating the shear forces transferred to the of boundary columns was also investigated. The strut width estimated as 0.243 m using Equation 2.6. The estimated strut width was again found to be considerably small compared to the strut width obtained from the analysis (0.75 m). Expected shear forces on boundary columns were also computed. The shear force transferred from the infill wall at the failure of the infill was estimated as 74.4 kN which is found to be small compared to the maximum shear demand on boundary columns obtained from the simulations (93 kN). Equation 2.8 and 2.9 were used to calculate the expected shear demand in case of a short column formation along the strut width and a shear demand of 125 kN was obtained. Shear demand based on short column effect, despite the fact that a short column formation was not observed, was found to be on the safe side for boundary column shear demand estimation.

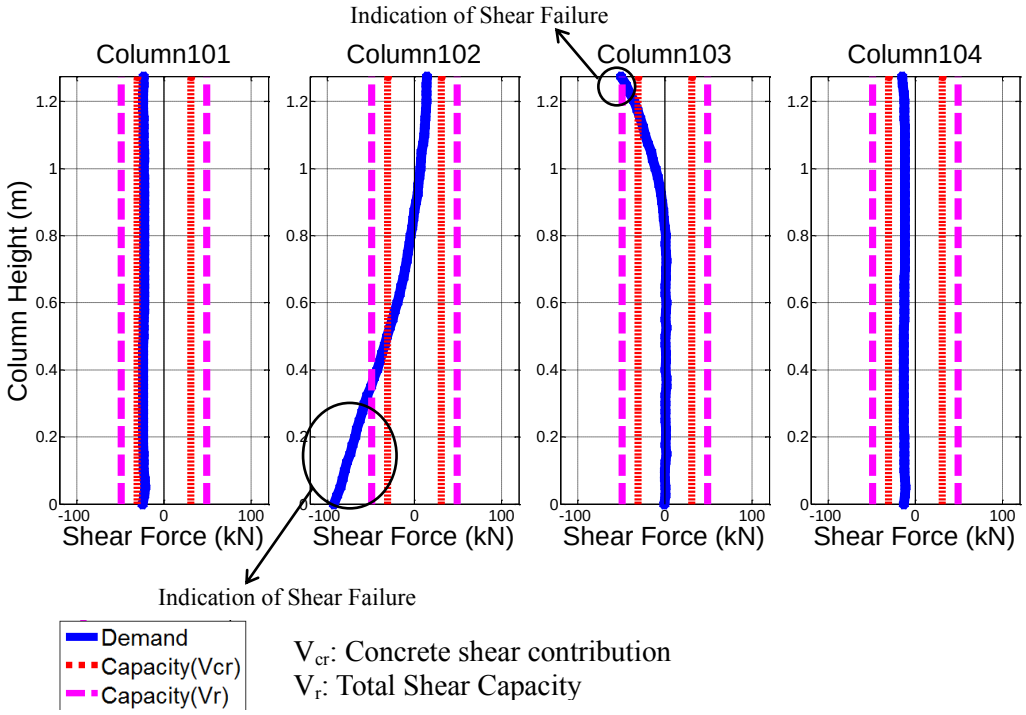

Figure 3.10: Shear Force Diagrams of the First Story Columns at Peak Deformation for Specimen 2

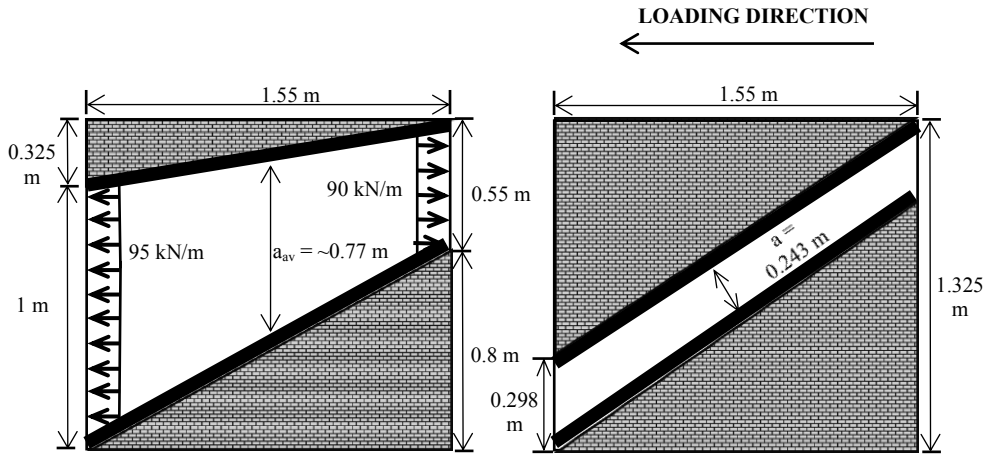

a) Simulation Results *b) ASCE/SEI 41-06 Estimation*

Figure 3.11: Properties of the Compression Strut for Specimen 2

3.6. Assessment Using ASCE/SEI 41-06 Guidelines

ASCE/SEI 41-06 is the only guideline providing assistance in seismic assessment and rehabilitation of reinforced concrete buildings with infill walls. The document is based on FEMA 356 (2000) and provides guidelines on assessment and rehabilitation of a wide range of building types. The assessment procedure consists of estimating deformation and force demands and comparing them with the performance limits provided for different performance levels. However, according to the report by EERI/PEER (2006), the deformation limits provided by ASCE/SEI 41-06 were found to be overly conservative. In 2007, a new document named ASCE/SEI 41 Supplement 1 was released and proposed updates on the provisions related to existing reinforced concrete buildings. These updates include revisions of modeling parameters and acceptance criteria for reinforced concrete beams, columns, beam-column joints and shear walls based on more recent experimental and analytical studies. However, no improvements were provided for the assessment of concrete buildings with infill walls, especially for columns adjacent to infill walls.

ASCE/SEI 41-06 with its supplement provides modeling parameters and acceptance criteria for the assessment and rehabilitation of existing reinforced concrete structures. The modeling parameters and numerical acceptance criteria provided for different members differ according to the expected failure mode and ductility. Each member is classified according to its shear demand, capacity and detailing as flexure, flexure-shear or shear (i.e., condition i, condition ii or condition iii). For the expected failure mode, performance limits for the member show change. Three discrete structural performance levels were defined by the document (Figure 3.12). These are namely “Immediate Occupancy” (IO), “Life Safety” (LS) and “Collapse Prevention” (CP) performance levels. They also define two structural performance ranges which will represent the damage states between the discrete performance levels. “Damage Control” (DC) structural performance range is defined as the continuous range between IO and LS performance levels whereas “Limited Safety” (LS) is defined as the range between LS and CP performance levels.

For the structural and nonstructural performance levels, criteria for satisfying the given performance levels are also given by the guidelines. For columns to satisfy IO performance level, only minor hairline cracking and limited yielding are allowed. No crushing should be present. For LS performance level, spalling and shear cracking in ductile columns and minor spalling of cover concrete in non-ductile columns are allowed. CP performance level is defined as extensive cracking and hinge formation in ductile members, limited cracking or splice failure in some non-ductile columns and severe damage in short columns.

Seismic assessment of the two test specimens was carried out according to the nonlinear procedure provided by ASCE/SEI-41-06 guidelines including the updates in 2007. For reinforced concrete buildings with infill walls, modeling parameters and acceptance criteria differs for the isolated columns and boundary columns. For isolated columns,

modeling parameters and acceptance criteria are defined in terms of plastic rotations where they are defined in terms of total average strain for the boundary columns. In the average strain based approach for boundary columns, the column members are considered as axial load carrying members and modeling of these members as truss elements is allowed. For the assessment of boundary columns, two approaches were followed in this study. The methods used for total strain along the length of the member and plastic hinge strains are addressed as “method 1” and “method 2”, respectively. It should be noted that the only difference between method 1 and 2 is the strain demand calculation. In method 1, strain demand is the average total strain along the column height, on the other hand, in method 2, strain demand within the plastic hinge zone (i.e. h/2 from column top and bottom) were considered while comparing with the strain limits provided by the guidelines. The previously mentioned numerical model which was proven to be successful in estimating the local demand parameters was used in the analysis without any modifications. Seismic assessment of all the beam and column members except boundary columns were conducted using the plastic rotation based method of ASCE/SEI 41-06. Column members adjacent to the infill walls in the central bay was evaluated according to the strain based numerical acceptance criteria given for reinforced concrete infilled frames in ASCE/SEI 41-06.

Observed damage at the first story columns and the infill wall at the end of the experiment for Specimen 1 are given in Figure 3.13. Considering the guidelines provided by ASCE/SEI 41-06 on determining the performance level of column members, the performance range based on visual observation for the boundary columns is considered limited safety (between LS and CP). On the other hand, exterior columns satisfied the life safety performance level and therefore considered to be in the damage control performance range /between IO and LS).

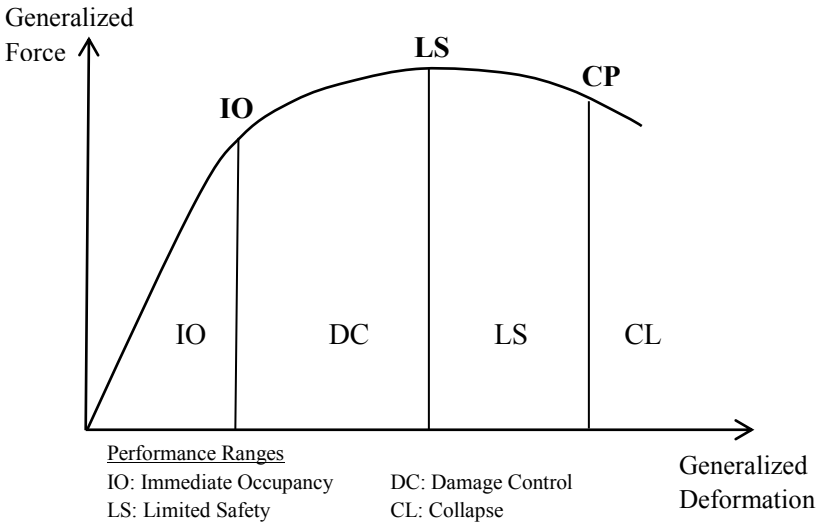

Figure 3.12: Performance Levels and Ranges

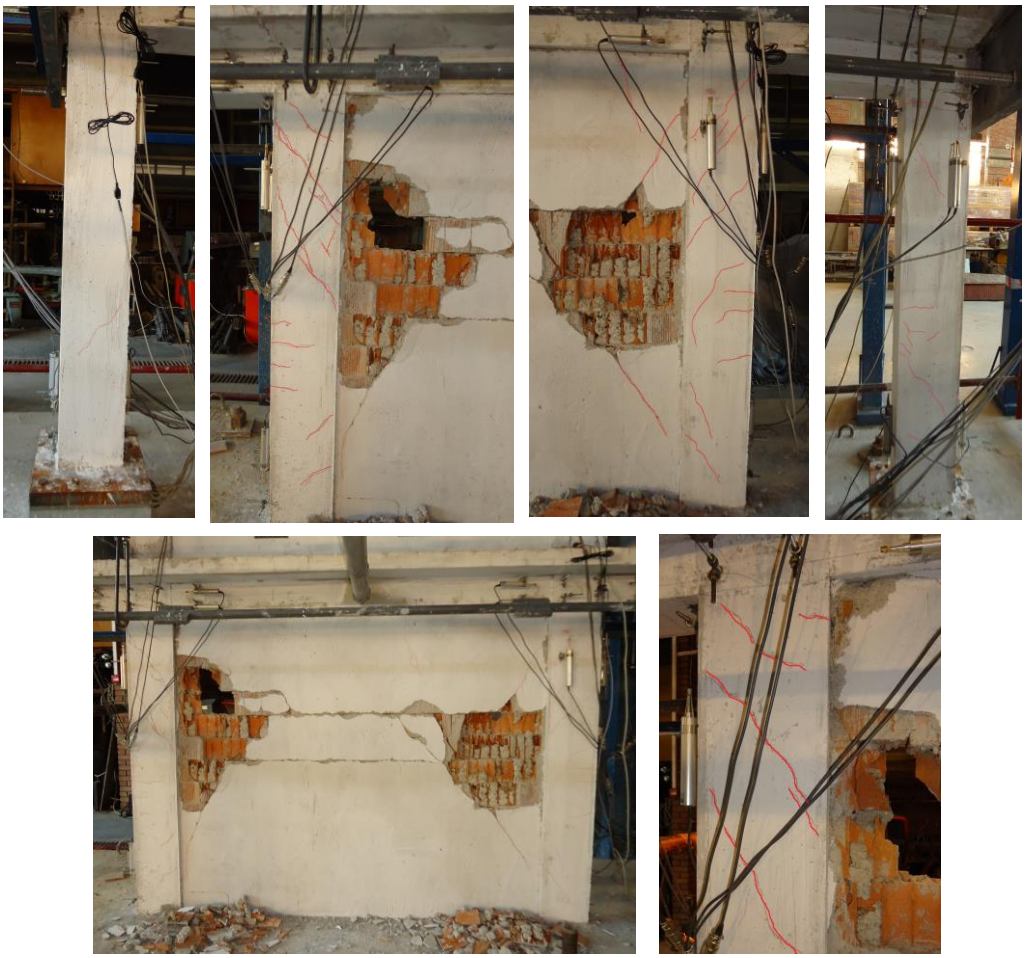

Figure 3.13: Observed Damage at the end of the Experiment for Specimen 1

For the seismically deficient frame (Specimen 2), observed damage regarding the first story columns and the infill wall are presented in Figure 3.14. Extensive shear damage was observed resulting in a significant decrease in the ductility of the members. Spalling of cover concrete and longitudinal bar buckling was observed in one of the boundary columns. Boundary columns are considered to go beyond collapse prevention performance level i.e. collapsed based on visual observation of the damage. Wide flexural cracks were observed at the bottom regions of the exterior columns, however spalling of the cover concrete or shear cracking was not observed. This implies that the exterior columns satisfied the life safety performance level (damage control performance range). It was also observed that the infill wall was nearly not damaged excluding some minor cracks near columns and crushing at one corner. Both in-plane strength and out-of plane stability of the infill wall was preserved after the experiment.

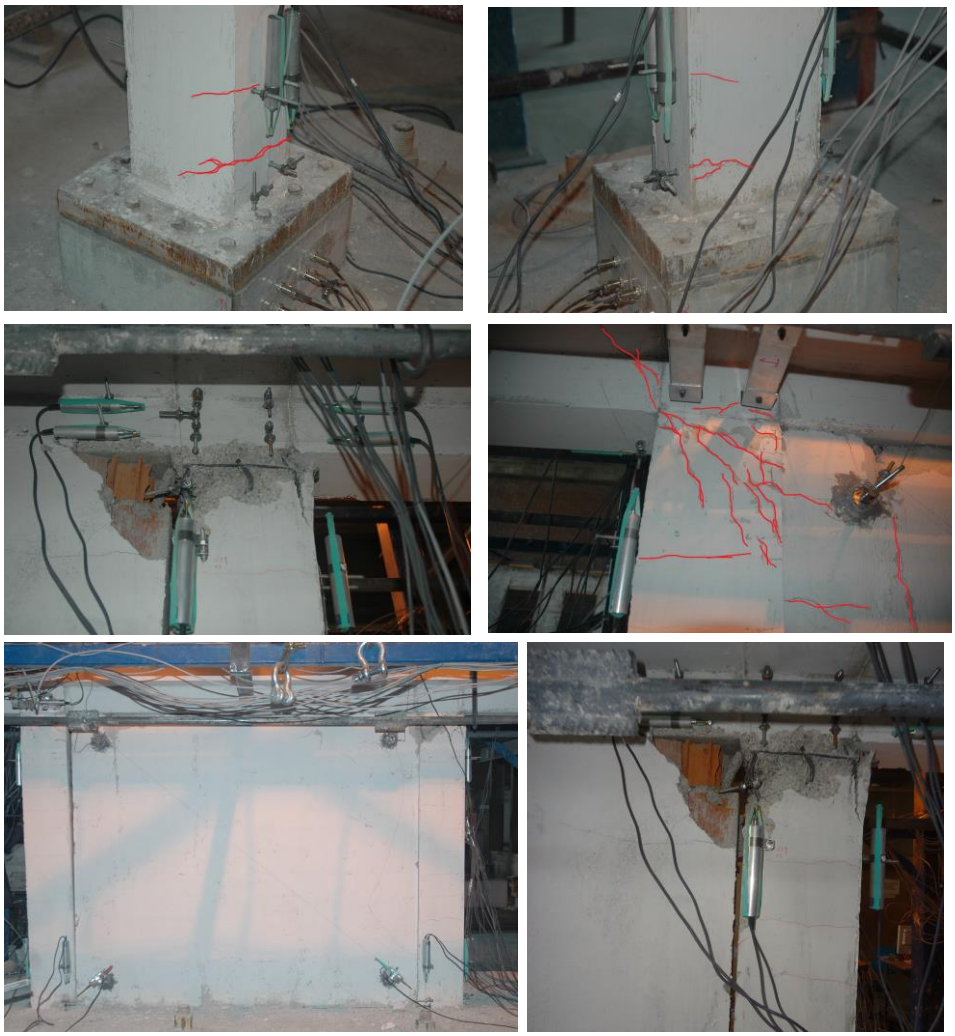

Figure 3.14: Observed Damage at the end of the Experiment for Specimen 2

Seismic assessment of the two frames was conducted using the two methods explained previously. The main focus of the assessment was to determine the accuracy of the methods in estimating the damage in boundary columns and all the other members. The first step in the assessment was to classify the members according to their expected failure mode. The criteria for classification according to ASCE/SEI 41-06 are presented in Table 3.3. For Specimen 1, all the members were classified as flexural members (i.e. condition i). For Specimen 2, since the shear detailing consisted of 90° closed hoops, all the members fell into flexure-shear failure mode (condition ii). Details of the classification are given in Table 3.4 and Table 3.5. Here, for Specimen 1, the shear strength of the RC frame members were calculated according to the formula provided by ACI 318 which is given as:

$$V_c = 0.17\left(1 + \frac{N_u}{14A_g}\right)\lambda\sqrt{f_c'}\,b_w d \quad (3.1)$$

$$V_w = \frac{A_{sw}}{s} f_{ywd} d \quad (3.2)$$

Where N_u is the axial load on the column and λ is a modification factor which can be taken as 1.0 for normal strength concrete. Other parameters were defined in Chapter 2. Shear demand for each member was calculated considering flexural hinge formations at both ends of the member.

Table 3.3: ASCE/SEI 41-06 Classification Criteria for Columns

	Transverse Reinforcement Details		
	ACI conforming details with 135 hooks	Closed hoops with 90 hooks	Other (including lap spliced transverse reinforcement)
Vp/(Vn/k)	i	ii	ii
1 ≥ Vp/(Vn/k) >0.6	ii	ii	iii
Vp/(Vn/k) > 1.0	iii	iii	iii

condition i: flexure failure, condition ii: flexure-shear failure, condition iii: shear failure

Vn: plastic shear capacity of the column, Vp: shear demand at flexural yielding of plastic hinges,

k: modifier for ductiliy

Table 3.4: Determination of the Expected Failure Mode for Columns of Specimen 1

	Member	V_p (kN)	V_n (kN)	$V_p/(V_n/k)$	Condition
First Story	Column 101	38.5	64.3	0.42	condition i
	Column 102	38.5	65	0.41	condition i
	Column 103	38.5	65	0.41	condition i
	Column 104	38.5	64.3	0.42	condition i
Second Story	Column 201	38.5	62.9	0.43	condition i
	Column 202	38.5	63.7	0.42	condition i
	Column 203	38.5	63.7	0.42	condition i
	Column 204	38.5	62.9	0.43	condition i
Third Story	Column 301	38.5	61.6	0.44	condition i
	Column 302	38.5	62.3	0.43	condition i
	Column 303	38.5	62.3	0.43	condition i
	Column 304	38.5	61.6	0.44	condition i

Table 3.5: Determination of the Expected Failure Mode for Columns of Specimen 2

	Member	V_p (kN)	V_n (kN)	$V_p/(V_n/k)$	Condition
First Story	Column 101	27.8	47	0.41	condition ii
	Column 102	27.8	47.6	0.41	condition ii
	Column 103	27.8	47.6	0.41	condition ii
	Column 104	27.8	47	0.41	condition ii
Second Story	Column 201	27.8	45.8	0.42	condition ii
	Column 202	27.8	46.5	0.42	condition ii
	Column 203	27.8	46.5	0.42	condition ii
	Column 204	27.8	45.8	0.42	condition ii
Third Story	Column 301	27.8	44.8	0.43	condition ii
	Column 302	27.8	45.3	0.43	condition ii
	Column 303	27.8	45.3	0.43	condition ii
	Column 304	27.8	44.8	0.43	condition ii

In light of the expected failure mode of the members, assessment of the isolated and boundary columns were conducted separately. The plastic rotation based procedure was applied for the exterior columns and the strain based method was applied for the boundary columns. As mentioned earlier, average total strain based assessment of the boundary columns were conducted considering two different approaches. Assessment results regarding columns and infill walls of Specimen 1 are presented in Figure 3.15. Since for both of the methods, all the members satisfied immediate occupancy performance level after D1 earthquake, assessment results are given for D2 and D4 earthquakes only.

For the D2 earthquake, damage states of the isolated columns were estimated accurately by the plastic rotation based method. For the boundary columns, when the average axial strain along the entire length of the member was considered, the strain limits provided by the guidelines were much larger than the strain demands. This resulted in unsafe estimations of the damage. Even for the D2 earthquake, boundary columns experienced minor shear cracking which could not be estimated by this procedure. On the other hand, using the plastic hinge strains at the boundary column ends gave conservative results. Assessment of the masonry infill walls was also conducted according to the drift based approach provided by the guideline. Performance levels in terms of inter-story drift ratios were given in Table 1.3. Infill wall damage at the first story was estimated correctly; however for the upper stories the damage was overestimated which can be attributed to the overestimation in inter-story drifts of the second and third stories in the analysis.

Same procedure was applied for the D4 earthquake and similar results were obtained. The plastic rotation based procedure concerning the exterior columns gave accurate estimations of damage state observed on those members. As discussed earlier, boundary columns were considered to pass the life safety performance level because of the ob-

served shear damage. Again, the observed damage could not be estimated by the two methods. Similar to the previous case (D2 earthquake), method 1 gave unsafe results and method 2 gave slightly conservative results. For the strain based procedure, unreasonable results were obtained for the second and third story boundary columns where no significant damage was observed in the experiment. Infill wall damage was also overestimated for the second and third stories whereas it was accurate for the first story.

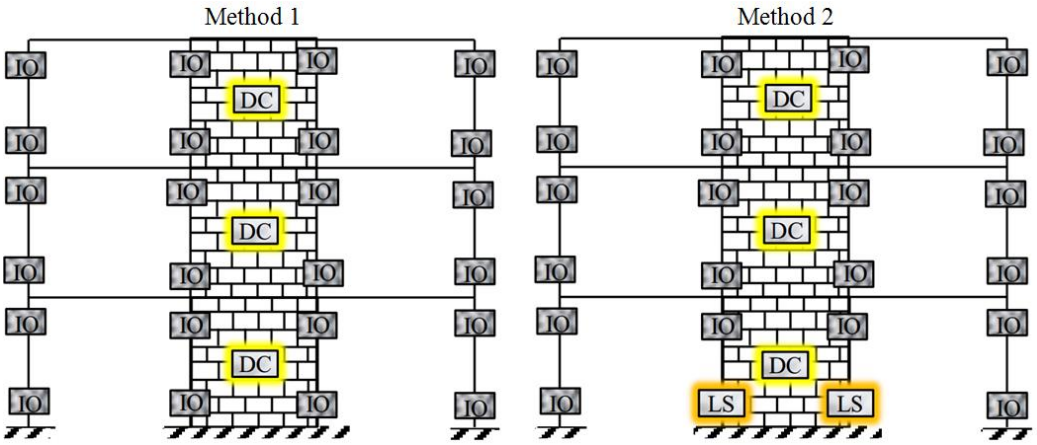

IO: Immediate Occupancy, DC: Damage Control, LS: Limited Safety, CL: Collapse

a) D2 Earthquake

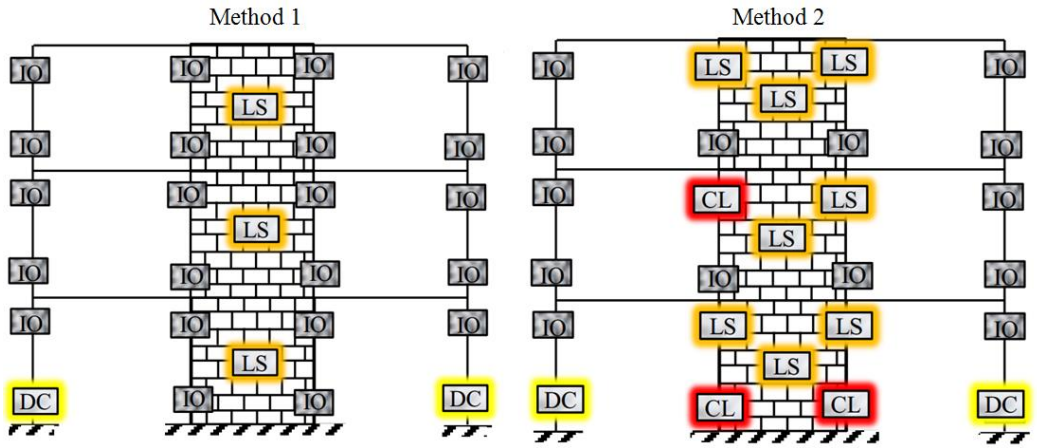

IO: Immediate Occupancy, DC: Damage Control, LS: Limited Safety, CL: Collapse

b) D4 Earthquake

Figure 3.15: Assessment Results for Specimen 1

Nonlinear seismic assessment of Specimen 2 was also conducted according to the ASCE/SEI 41-06 guidelines. The results of the assessment for D2 and D4 earthquakes are given in Figure 3.16. Since all the members satisfied immediate occupancy performance level for D1 earthquake, results regarding that ground motion are not given. Assessment results for the D2 earthquake was exactly the same as Specimen 1. Again, damage states of the isolated columns were estimated accurately by the plastic rotation based method. At the D2 earthquake visible shear cracks were observed at the first story columns. This damage state was captured by method 2, however method 1 failed to capture the shear induced damage on the structure.

For D4 earthquake, the exterior columns were found to satisfy the life safety performance level according to the assessment results. This result is compatible with the observed damage as addressed earlier in this study. As in the case of the code conforming frame, both methods used for the boundary column assessment failed to capture the actual response. Using total strain along the entire length exhibited extremely unsafe results and using plastic hinge strains caused overestimation of the damage for some members, similar to the code conforming specimen.

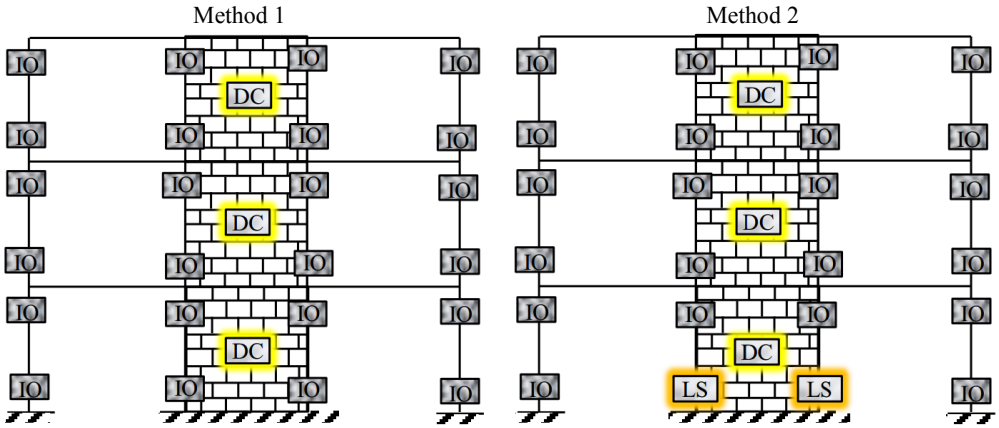

IO: Immediate Occupancy, DC: Damage Control, LS: Limited Safety, CL: Collapse

a) D2 Earthquake

Figure 3.16: Assessment Results for Specimen 2 (cont'd)

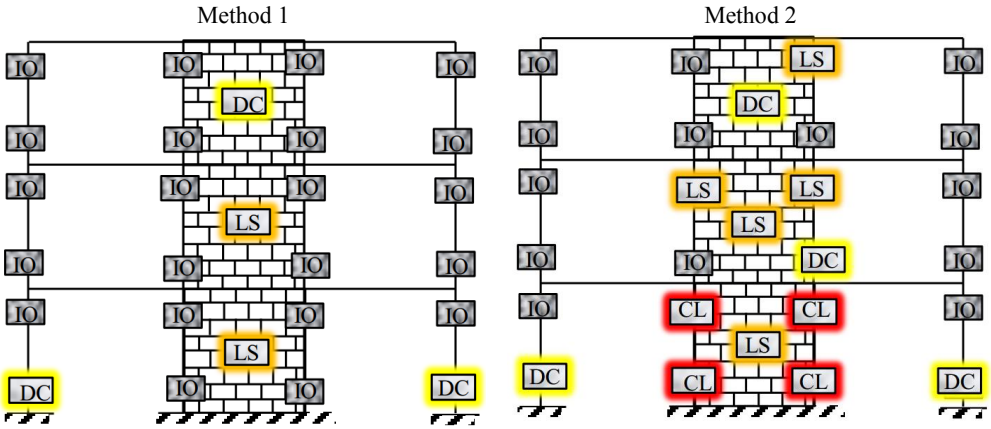

IO: Immediate Occupancy, DC: Damage Control, LS: Limited Safety, CL: Collapse

b) D4 Earthquake

Figure 3.16: Assessment Results for Specimen 2 (cont'd)

Furthermore, bar charts for both specimens representing the plastic rotations calculated for each column end is given (Figure 3.17 and Figure 3.18) along with the performance limits for the members. By the use of bar charts, accuracy of estimations on member damage can be better illustrated. Once again, it can be observed that the damage states of the isolated columns were accurately predicted with the plastic rotation based procedure. Plastic rotations of boundary column ends are also included in the charts. It is clear that, for the code conforming specimen, the rotation based procedure cannot be used to estimate damage on those members since the shear demand on the members could not be determined accurately by the current procedure which does not account for the forces transferred from the infill walls. Shear demand was calculated considering plastic hinging at the two column ends according to the procedure; however it was shown that the actual shear demand was larger. For the seismically deficient specimen, same procedure exhibited better estimations on boundary column damage, however failed to predict the actual failure mode (shear failure).

Compressive and tensile strains of boundary columns obtained with the two methods are also presented (Figure 3.19 and Figure 3.20). It is shown that both the degree of underestimation in case of method 1 and the degree of overestimation in case of method 2 were dramatic. Considering both the average strain values and plastic hinge strain values obtained for boundary columns, strain based procedure was not found to be effective with the given limits in the assessment of boundary columns.

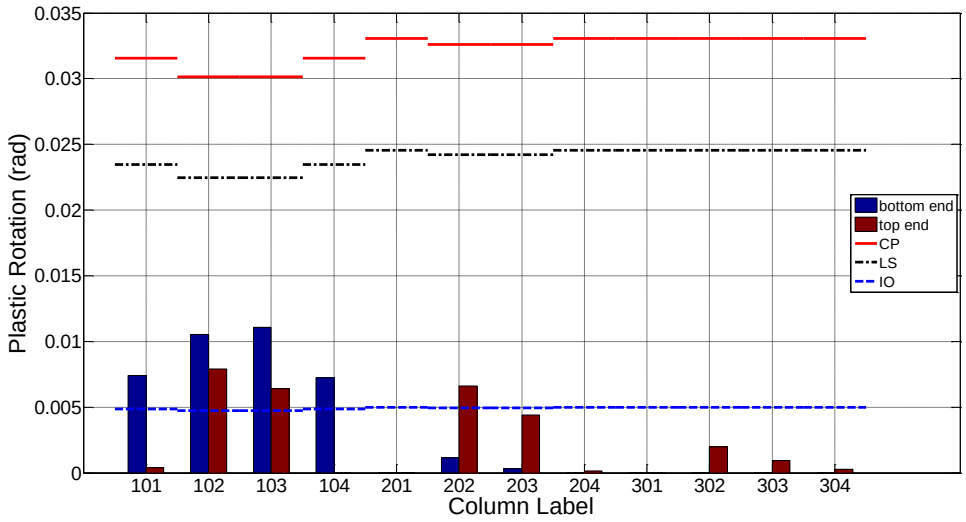

Figure 3.17: Plastic Rotations and Performance Limits for Columns of Specimen 1

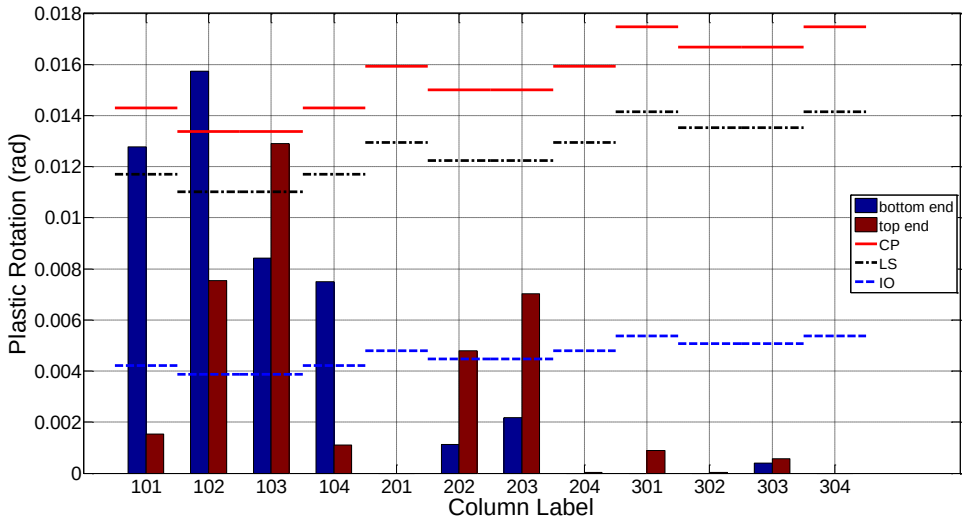

Figure 3.18: Plastic Rotations and Performance Limits for Columns of Specimen 2

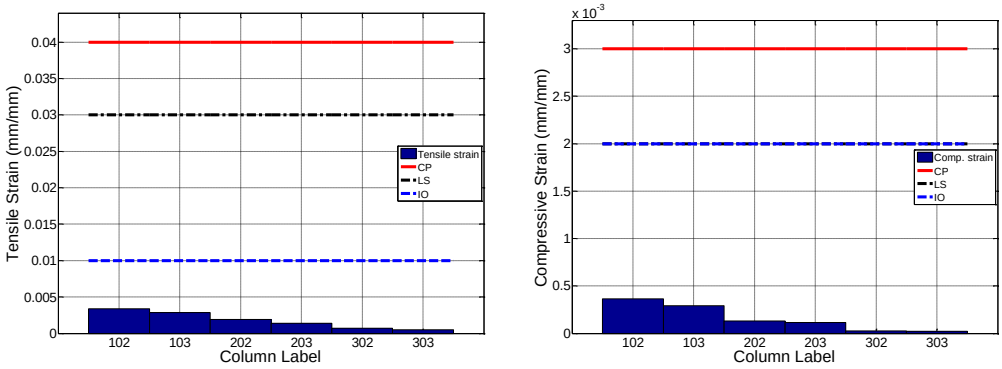

a) Maximum Average Strain along the Length of Columns (Method 1)

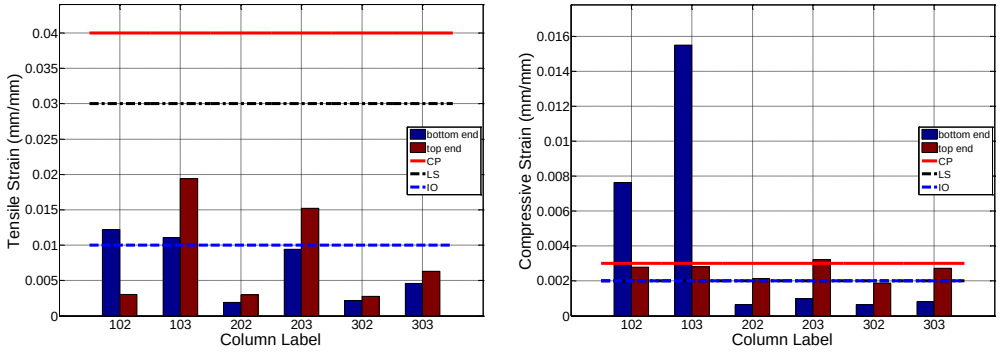

b) Maximum Plastic Hinge Strain (Method 2)

Figure 3.19: Tensile and Compressive Strains at Boundary Columns of Specimen 1

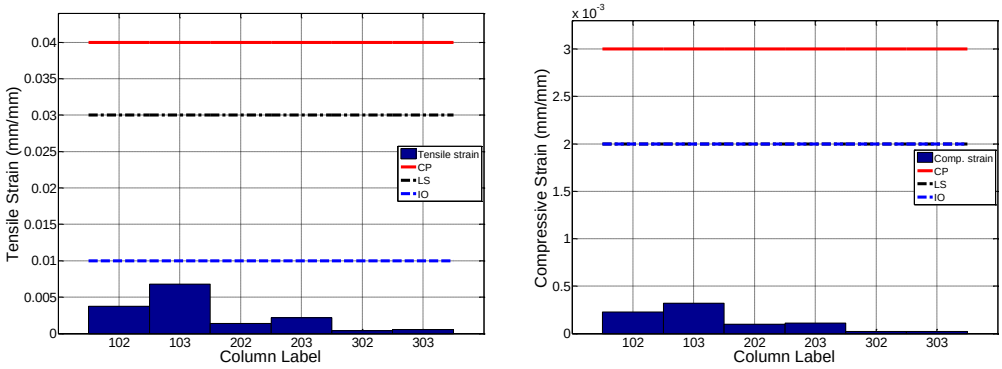

a) Maximum Average Strain along the Length of Columns (Method 1)

Figure 3.20: Tensile and Compressive Strains at Boundary Columns of Specimen 2 (cont'd)

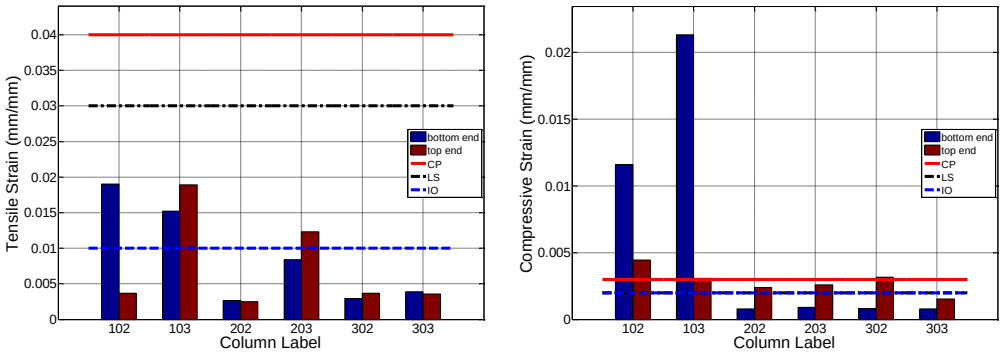

b) Maximum Plastic Hinge Strain (Method 2)

Figure 3.20: Tensile and Compressive Strains at Boundary Columns of Specimen 2 (cont'd)

In order to further elaborate on the accuracy of the available methods for the assessment of the boundary columns in reinforced concrete frames with URM infill walls, nonlinear assessment of the 9 test specimens of Mehrabi (1994) was conducted. The pushover analyses which were conducted to validate the proposed finite element modeling approach were used in the assessment. Results of the pushover analyses were found satisfactory in terms of estimating global demand parameters. For all specimens, 20 % capacity drop was considered as "collapse". Nonlinear assessment of the specimens were conducted at the points on the pushover curves corresponding to a capacity drop of 20% and members were expected to pass the collapse prevention performance level. Results for each specimen are provided in Table 3.6. In the light of the assessment results for the two methods, it is clear that method 1 failed to estimate the correct damage state and gave extremely unsafe results where the accuracy of method 2 was acceptable.

Table 3.6: Assessment Results for Test Specimens of Mehrabi (1994)

	Method 1		Method 2			
	Column 101	Column 102	Column 101		Column 102	
			bottom	top	bottom	top
Specimen2	IO	IO	CL	CL	CL	CL
Specimen3	IO	IO	CL	CL	CL	IO
Specimen4	IO	IO	CL	LS	CL	CL
Specimen5	IO	IO	CL	LS	CL	IO
Specimen6	IO	IO	CL	CL	CL	CL
Specimen7	IO	IO	CL	CL	CL	IO
Specimen8	IO	IO	CL	CL	CL	CL
Specimen9	IO	IO	CL	CL	CL	IO
Specimen10	IO	IO	CL	CL	CL	CL

IO: Immediate Occupancy, DC: Damage Control, LS: Limited Safety, CL: Collapse

CHAPTER 4

CONCLUSIONS

Investigation of the seismic behavior and performance of boundary columns in reinforced concrete frames with URM infill walls is presented in the course of this thesis. Experimental results regarding pseudo dynamic tests on a code conforming frame designed according to TEC (2007) and a deficient frame were presented and interpreted. A numerical modeling approach was developed using the available constitutive models and validated with experiments. Nonlinear time history analyses of the test specimens were carried out using the validated numerical modeling approach and compared with the experimental results. Using the analysis results, compressive strut width and magnitude of the uniform distributed load imposed on columns were calculated. Additionally, seismic performance assessments of the test specimens were conducted according to ASCE/SEI 41-06 guidelines using the simulation results. For the evaluation of boundary columns, two methods were considered. In the first method which was proposed by the guidelines, total axial compressive and tensile strains along the column length was considered whereas in the second method, plastic hinge strains was calculated and compared with the limits provided by the guidelines.

The following conclusions are extracted in light of the experimental and analytical study:

- The seismic behavior of reinforced concrete frames is significantly altered by the presence of infill walls. Stiffness, strength, deformation capacity, ductility and failure modes of such structures are affected greatly by the frame-infill wall interaction. Substantial amount of shear force is transferred from infill walls to the boundary columns in the form of a uniform distributed load along the strut width. This results in shear damage on boundary column members and prevents the ductile behavior.

- Detrimental effects of the infill walls on boundary columns are found to be more critical in case of weak frames and strong infill walls. Strong infill walls can transfer more load to the boundary frame without any horizontal sliding or diagonal cracking failure as the story drifts increase. Nevertheless, the effects are

still dangerous in case of strong frames since the ductility of the member is limited by the shear damage.

- Global demand parameters such as inter-story drift ratios and base shear capacity are estimated with about 30% certainty with the most sophisticated methods available to the engineers in practice. Continuum modeling of the infill wall is found satisfactory in terms of estimating the global behavior and the shear damage on boundary columns. However, local demand parameters are found difficult to estimate even with continuum modeling.

- The forces transferred from the infill wall to the boundary columns should be considered in both design and performance assessment of such buildings. The capacity design principle which is used by TEC (2007) is found unsatisfactory for the frames investigated in this study, considering the safety of the boundary columns. It is advised that shear design of such columns should be made considering the shear forces transferred from the infill walls.

- Guidelines provided by ASCE/SEI 41-06 exhibits accurate estimations regarding isolated columns, however the strain based methods provided for the assessment of boundary columns are found to be extremely unsafe, lacking consistency and precision. When the strain limits are considered for plastic hinge strains at the member-ends, procedure gives safer results and stays at the conservative side.

REFERENCES

ACI Committee 318, 2008. “Building Code Requirements for Structural Concrete (ACI 318-08) and Commentary,” American Concrete Institute, Farmington Hills, MI

Akın, E., 2011. “Behavior of Brick Infilled Reinforced Concrete Frames Strengthened by CFRP Reinforcement- GENERAL PRINCIPLES”. Phd Thesis. METU

American Society of Civil Engineers, 2006. “Seismic Rehabilitation of Existing Buildings”, ASCE/SEI 41-06, Reston, Virginia

American Society of Civil Engineers, 2007. “Seismic Rehabilitation of Existing Buildings: Supplement #1”, ASCE/SEI 41-06:, Reston, Virginia.

Baran, M. & Sevil, T., 2010. “Analytical and Experimental Studies on Infilled RC Frames”. International Journal of the Physical Sciences. Vol. 5(13), pp. 1981-1998.

Bertero, V. & Brokken, S., 1983. “Infills in Seismic Resistant Buildings”. J. Struct. Eng. (ASCE), pp. 1337-1361.

Canbay, E., Ersoy, U., Tankut, T., 2004. A three-component Force Transducer for RC Structural Testing, Engineering Structures, 26(2), 257-265.

CEN European Standard EN 1998-1, 2004. Eurocode 8: Design of Structures for Earthquake Resistance, Part 1: General Rules, Seismic Actions and Rules for Buildings, Comitee Europeen de Normalisation, Brusells.

DIANA: Displacement Analyses, TNO DIANA, Delft, Netherlands, 2008.

EERI/PEER, 2006. “New Information on the Seismic Performance of Existing Concrete Buildings”, Seminar Notes:, Earthquake Engineering Research Institute, Oakland, California.

El-Dakhakni, W.W., Elgaaly, M., Hamid, A.A., 2003. “Three-strut model for concrete masonry-infilled steel frames,” ASCE J. of Struct. Eng.Vol. 129, No. 2, pp. 177-185.

Fardis, M.N., Bousias, S.N., Franchioni, G., Panagiotakos, T.B., 1999. “Seismic response and design of RC structures with plan-eccentric masonry infills,” Earthq. Eng. Struct. D.Vol. 28, No. 2, pp. 173-191.

Federal Emergency Management Agency, 2000. “Prestandard and Commentary for the Seismic Rehabilitation of Buildings”, FEMA (Series) 356, Washington, D.C.

Fiorato, A.E., Sozen, M.A., and Gamble, W.L., 1970. "An investigation of the interaction of reinforced concrete frames with masonry filler walls." Technical Report No. UILU-ENG 70-100, University of Illinois, Urbana-Champaign, IL.

Klingner, R. E., & Bertero, V.V., 1978. “Earthquake resistance of infilled frames,” J. of the Struct. Div., ASCE Vol. 104, No. ST6, 1978, pp. 973-989.

Koutromanos, I., 2011. “Numerical Analysis of Masonry-Infilled Reinforced Concrete Frames Subjected to Seismic Loads and Experimental Evaluation of Retrofit Techniques”, PhD Thesis: University of California, San Diego, Print.

Kurt, E. G., Binici, B., Kurç, Ö., Canbay, E., Akpınar, U., & Özcebe, G., 2011. Seismic Performance of a Deficient Reinforced Concrete Test Frame with Infill Walls. Earthquake Spectra, Volume 27(No.3), pp. 817-834.

Maia, N.M.M., and Silva, J.M.M., 1997. Theoretical and Experimental Modal Analysis, Research Studies Press, John Wiley.

Marjani, F., and Ersoy, U., 2002. “Behavior of Brick Infilled RC Frames Under Reserved Cyclic Loading”, ECAS 2002 International Symposium on Structural and Earthquake Engineering, Oct. 14.

Mehrabi, A. B., Shing, P. B., Schuller, M. P., & Noland, J. L., 1994. Performance of Masonry-Infilled R/C Frames Under In-Plane Lateral Loads. University of Colorado at Boulder, Dept. of Civil Envir. and Arch. Engineering. Colorado: Structural Engineering and Structural Mechanics Research Series.

Memari, A. M., & Aliaari, M., 2004. Seismic Isolation of Masonry Infill Walls. Structures (ASCE).

Middle East Technical University., 2010. “108G084 Tübitak Project Progress Report #1”. Aug. 5, Print.

Ministry of Public Works and Settlement, 2007. Turkish Code for Buildings in Seismic Zones, Ankara, Turkey, 159 (In Turkish).

Molina, F.J., Pegon, P., and Verzeletti, G., 1999. Time-domain identification from seismic pseudodynamic test results on civil engineering specimens, 2nd International Conference on Identification in Engineering Systems, University of Wales, Swansea, March 29-31.

Molina, F.J., Verzeletti, G., Magonette, G., Buchet, P.H., Géradin, M., 1999. Bi-Directional pseudodynamic test of a full-size three-storey building, Earthquake Engineering and Structural Dynamics, 28(12), 1541-1566.

Mosalam, K. M., & Hashemi, A., 2007. Seismic Evaluation of Reinforced Concrete Buildings Including Effects of Masonry Infill Walls. PEER Technical Report.

Mosalam, K. M., White, R. N., & Ayala, G., 1998. Response of Infilled Frames Using Pseudo-Dynamic Experimentation. Earthquake Engineering and Structural Dynamics, 27, pp. 589-608.

Mutlu, M.B., 2012. “Numerical Simulations of Reinforced Concrete Frames Tested using Pseudo-Dynamic Method”, Graduate Thesis: Middle East Technical University, Print.

Okuyucu, D., 2011. “Effects of Frame Aspect Ratio on the Seismic Performance Improvement of Panel Strengthening Technique”, Ph.D. Thesis: Middle East Technical University, Print.

Özcebe, G.Ö., Ersoy, U., Tankut, T., Erduran, E., Keskin, R.S.O., Mertol, H.C., 2003. "Strengthening of Brick-Infilled RC Frames with CFRP" Technical Report, Structural Engineering Research Unit, TÜBİTAK - METU.

Selby, R.G., and Vecchio, F.J., 1993. Three dimensional constitutive relations for reinforced concrete. Department of Civil Engineering, University of Toronto, Toronto, Ont., Publication No. 93-02.

Sozen, M. A., Fiorato, A. E., & Gamle, W. L., 1970. An Investigation of the Interaction of Reinforced Concrete Frames with Masonry Filler Walls. University of Illinois , Department of Defense, Urbana, Illinois.

Stavridis, A., Shing, P.B., 2010. “Finite element modeling of nonlinear behaviour of masonry-infilled RC frames,” ASCE J. Struct. Eng.Vol. 136, No. 3, pp. 285-296.

Takanashi, K., Udagawa, K., Seki, M., Okada, T., and Tanaka H., 1975. “Nonlinear earthquake response analysis of structures by a computer-actuator on-line system” Bulletin of Earthquake Resistant Structure Research Center 8, Institute of Industrial Science, University of Tokyo, Japan.

Vecchio F.J. and Collins M.P., 1993. Compression Response of Cracked Reinforced Concrete. Journal of Structural Engineering, ASCE, Volume119, No. 12: 3590-3610.